arXiv:1409.1467v1 [cs.IT] 4 Sep 2014

Evaluation of Position-related Information in Multipath Components for Indoor Positioning

Erik Leitinger*, Paul Meissner*, Christoph Ruedisser*, Gregor Dumphart*, and Klaus Witrisal*
* Graz University of Technology, Austria

***Abstract*—Location awareness is a key factor for a wealth of wireless indoor applications. Its provision requires the careful fusion of diverse information sources. For agents that use radio signals for localization, this information may either come from signal transmissions with respect to fixed anchors, from cooperative transmissions in between agents, or from radar-like monostatic transmissions. Using a-priori knowledge of a floor plan of the environment, specular multipath components can be exploited, based on a geometric-stochastic channel model. In this paper, a unified framework is presented for the quantification of this type of position-related information, using the concept of equivalent Fisher information. We derive analytical results for the Cramér-Rao lower bound of multipath-assisted positioning, considering bistatic transmissions between agents and fixed anchors, monostatic transmissions from agents, cooperative measurements in-between agents, and combinations thereof, including the effect of clock offsets and missing synchronization. Awareness of this information enables highly accurate and robust indoor positioning. Computational results show the applicability of the framework for the characterization of the localization capabilities of some environment, quantifying the influence of different system setups, signal parameters, and the impact of path overlap.**

I. Introduction

Location awareness is a key component of many future wireless applications. Achieving the needed level of accuracy *robustly* is still elusive, especially in indoor environments which are characterized by harsh multipath conditions. Promising candidate systems thus either use sensing technologies that provide remedies against multipath or they fuse information from multiple information sources [1], [2]. *Multipath-assisted indoor positioning* employs both of these strategies. Ultra-wideband (UWB) signals are used to facilitate the separation of multipath components (MPCs). Knowing the floor plan, these MPCs can be associated to the local geometry and used as additional (virtual) anchors (VAs). In this way, additional position-related information is exploited that is contained in the radio signals.

This is in contrast to competing approaches, which either detect and avoid non-line-of-sight (NLOS) measurements [3], mitigate errors induced by strong multipath conditions [4], or employ more realistic statistical models for the distribution of the range estimates [5]. Cooperation between agents is another method to increase the amount of available information [6] and thus to reduce the localization outage. Actual exploitation of multipath propagation requires prior knowledge [7]. This can be the floor plan, like in this work and related approaches [8], or a set of known antenna locations to enable beamforming (e.g. in imaging [9]). In an inverse problem, the room geometry can be inferred from the multipath and known measurement locations [10].

This work was supported by the Austrian Science Fund (FWF) within the National Research Network SISE project S10610, by the Austrian Research Promotion Agency (FFG) within KIRAS PL3, grant no. 832335 "LOBSTER", and by EU FP7 Marie Curie Initial Training Network MULTI-POS (Multi-technology Positioning Professionals) under grant nr. 316528.

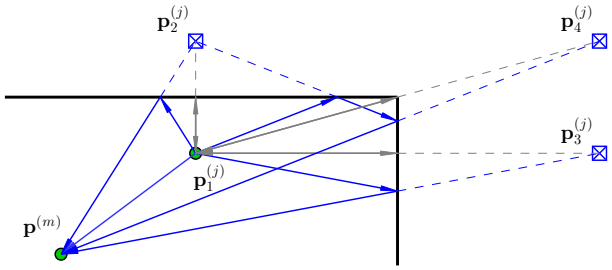

Fig. 1. Illustration of multipath geometry using VAs for (i) bistatic transmissions (blue) between an anchor at $\mathbf{p}_1^{(j)}$ and an agent at $\mathbf{p}^{(m)}$ and for (ii) a monostatic measurement (gray) by an agent at $\mathbf{p}_1^{(j)}$.

Insight on the position-related information that is conveyed in the signals [11] can be gained by an analysis of performance bounds. Using the concept of equivalent Fisher Information Matrices (EFIMs) [12], [13], allows for analytic evaluation of the Cramér-Rao lower bound (CRLB) for vector parameters by blockwise inversion of the FIM [14]. A proper channel model is paramount to capture the information contained in MPCs. For instance in [12], the arrival angles of MPCs are not considered, hence each signal provides information along the direction from the anchor to the agent only. Propagation effects other than the geometrically modeled MPCs constitute interference to useful position-related information. These effects are often subsumed in a term called diffuse multipath (DM) [15] and modeled statistically. Its detrimental influence can be evaluated by a whitening operation [16] that accounts for its non-stationary statistics. Channel models that include DM [17]–[21] can model the propagation behavior in an environment more realistically than models that just rely on deterministic effects. Such models are often referred to as hybrid geometric-stochastic channel models (GSCMs). Our prior work in [22]–[24] has shown the significant performance gain that can be achieved using awareness of these components.

Fig. 1 illustrates the geometric model for multipath-assisted positioning. A signal transmitted between an anchor at position $\mathbf{p}_1^{(j)}$ and an agent at $\mathbf{p}^{(m)}$ includes specular reflections at the

room walls, indicated by the blue lines.[1] These reflections can be modeled geometrically using VAs $\mathbf{p}_{\mathrm{k}}^{(j)}$, mirror images of the anchor w.r.t. walls that can be computed from the floor plan [22], [25], [26]. We call this the *bistatic* setup, where the fixed anchors and the floor plan constitute the available infrastructure. In a *cooperative* setup, agents localize themselves using bistatic measurements in between them. Here, the node at $\mathbf{p}_1^{(j)}$ is an agent that plays the role of an anchor (and thus provides a set of VAs) for the agent at $\mathbf{p}^{(m)}$. If the agents are equipped accordingly, they can use *monostatic* measurements, indicated by the gray lines. Here, the node at $\mathbf{p}_1^{(j)}$ acts as anchor for itself with its own set of VAs.

For these measurement setups, we identity the following scenarios of interest: (i) Multipath-ToA (time of arrival) with known synchronization between anchors and agents, (ii) Multipath-TDoA (time difference of arrival) with unknown synchronization between either anchors and agents or also between the individual anchors, and (iii) Multipath-Coop with cooperation between the anchors, monostatic measurements, and possibly additional fixed anchors. For a tracking application, we have coined the terms *multipath-assisted indoor navigation and tracking (MINT)* for the bistatic setup [15], and Co-MINT [27] for the cooperative setup. The robustness and accuracy of MINT have been reported in [22]–[24] and references therein. Also, a real-time demonstration system has been realized [23].

The key contributions of this paper are:

- We present a mathematical framework for the quantification of position-related information contained in geometrically modeled specular reflections in (ultra) wideband wireless signals under DM.
- This information is quantified for conventional bistatic, monostatic, and cooperative measurement scenarios, optionally including unknown clock offsets, allowing for important insights that can be used in the design of a localization system.
- The results show the relevance of a site-specific, position-related channel model for indoor positioning and the components it comprises of.

The paper is organized as follows: Section II introduces the geometric-stochastic signal model that is used in Section III to derive the CRLB on the position estimation error. Section IV describes the relationship between signal parameters and node positions in a generic form. These results are used in Section V to derive the CRLB for the different scenarios. Finally, Sections VI and VII wrap up the paper with results, discussions, and conclusions.

Mathematical notations: $\mathbb{E}_z\{\cdot\}$ represents the expectation operator with respect to the random variable z. $\mathrm{tr}\{\cdot\}$ and $\mathrm{diag}\{\cdot\}$ are the trace and the diagonal of a square matrix, respectively. $[\mathbf{A}]_{n,m}$ is the (n,m)-th element of matrix $\mathbf{A}$; $\mathbf{A}_{N\times M}$ indicates the size of a matrix. $\|\cdot\|$ is the Euclidean norm, $|\cdot|$ is the absolute value, and $(*)$ denotes convolution. $\mathbf{A}\succeq\mathbf{B}$ means that $\mathbf{A}-\mathbf{B}$ is positive semidefinite. $\mathbf{I}_N$ is the identity matrix of size N. $(\cdot)^{\mathrm{H}}$ is the Hermitian conjugate.

[1]Since the radio channel is reciprocal, the assignment of transmitter and receiver roles to anchors and agents is arbitrary and this choice can be made according to higher-level considerations.

II. Signal Model

In Sections II and III, we simplify the setup—for the ease of readability—to a single (fixed) anchor located at position $\mathbf{p}_1\in\mathbb{R}^2$ and one agent at position $\mathbf{p}\in\mathbb{R}^2$. Note that two-dimensional position coordinates are used throughout the paper, for the sake of simplicity. A *baseband* UWB signal $s(t)$ with effective pulse duration T_p is exchanged between the anchor and the agent. The corresponding received signal is modeled as [15]

$$\begin{aligned} r(t) &= r_{\mathrm{det}}(t) + r_{\mathrm{diff}}(t) + w(t) \\ &= \sum_{k=1}^{K} \alpha_k s(t-\tau_k) + (s*\nu)(t-\epsilon) + w(t). \end{aligned} \tag{1}$$

The first term $r_{\mathrm{det}}(t)$ describes a sum of K deterministic MPCs with complex amplitudes $\{\alpha_k\}$ and delays $\{\tau_k\}$. We model these delays by VAs at positions $\mathbf{p}_k\in\mathbb{R}^2$, yielding $\tau_k=\frac{1}{c}\|\mathbf{p}-\mathbf{p}_k\|+\epsilon$, with $k=1\ldots K$, where c is the speed of light and ϵ represents the clock-offset due to clock asynchronism. K is equivalent to the number of visible VAs at the agent position $\mathbf{p}$ [22]. We assume the energy of $s(t)$ is normalized to one.

The second term $r_{\mathrm{diff}}(t)$ denotes the convolution of the transmitted signal $s(t)$ with the DM $\nu(t)$, which is modeled as a zero-mean Gaussian random process. We assume uncorrelated scattering along the delay axis τ, hence the autocorrelation function (ACF) of $\nu(t)$ is given by

$$K_\nu(\tau,u)=\mathbb{E}_\nu\{\nu(\tau)\nu^*(u)\}=S_\nu(\tau)\delta(\tau-u), \tag{2}$$

where $S_\nu(\tau)$ is the power delay profile (PDP) of DM at the agent position $\mathbf{p}$. The DM process is assumed to be quasi-stationary in the spatial domain, which means that $S_\nu(\tau)$ does not change in the vicinity of position $\mathbf{p}$ [28].

Finally, the last term $w(t)$ denotes an additive white Gaussian noise (AWGN) process with double-sided power spectral density (PSD) of $N_0/2$.

In the following, we will drop the clock-offset ϵ. We will re-introduce it in SectionV-B where the TDoA measurement scenario is studied.

III. Cramér-Rao Lower Bound

The goal of multipath-assisted indoor positioning is to estimate the agent's position $\mathbf{p}$ from the signal waveform (1), exploiting the knowledge of the VA positions $\{\mathbf{p}_k\}$, in presence of diffuse multipath and AWGN with known statistics. Let $\hat{\boldsymbol{\theta}}$ denote the estimate of the position-related parameter vector $\boldsymbol{\theta}=[\mathbf{p}^{\mathrm{T}}\ \Re\boldsymbol{\alpha}^{\mathrm{T}}\ \Im\boldsymbol{\alpha}^{\mathrm{T}}]^{\mathrm{T}}\in\mathbb{R}^{D_{\boldsymbol{\theta}}}$, where $\Re\boldsymbol{\alpha}=[\Re\alpha_1,\ldots,\Re\alpha_K]^{\mathrm{T}}$ and $\Im\boldsymbol{\alpha}=[\Im\alpha_1,\ldots,\Im\alpha_K]^{\mathrm{T}}$ are the real and imaginary parts of the complex amplitudes $\boldsymbol{\alpha}$, respectively, which are nuisance parameters. According to the information inequality, the error covariance matrix of $\boldsymbol{\theta}$ is bounded by

$$\mathbb{E}_{\mathbf{r}|\boldsymbol{\theta}}\left\{\left(\hat{\boldsymbol{\theta}}-\boldsymbol{\theta}\right)\left(\hat{\boldsymbol{\theta}}-\boldsymbol{\theta}\right)^{\mathrm{H}}\right\}\succeq\boldsymbol{\mathcal{I}}_{\boldsymbol{\theta}}^{-1}, \tag{3}$$

where $\boldsymbol{\mathcal{I}}_{\boldsymbol{\theta}} \in \mathbb{R}^{D_{\boldsymbol{\theta}} \times D_{\boldsymbol{\theta}}}$ is the Fisher information matrix (FIM) and its inverse represents the CRLB of $\boldsymbol{\theta}$. We apply the chain rule to derive this CRLB (cf. [12], [14]), i.e., the FIM $\boldsymbol{\mathcal{I}}_{\boldsymbol{\theta}}$ is computed from the FIM of the signal parameter vector $\boldsymbol{\psi} = \left[\boldsymbol{\tau}^{\mathrm{T}}, \Re\boldsymbol{\alpha}^{\mathrm{T}}, \Im\boldsymbol{\alpha}^{\mathrm{T}}\right]^{\mathrm{T}} \in \mathbb{R}^{D_{\boldsymbol{\psi}}}$, where $\boldsymbol{\tau} = [\tau_1, \ldots, \tau_K]^{\mathrm{T}}$ represents the vector of position-related delays. We get

$$\boldsymbol{\mathcal{I}}_{\boldsymbol{\theta}} = \mathbf{J}^{\mathrm{T}} \boldsymbol{\mathcal{I}}_{\boldsymbol{\psi}} \mathbf{J} \tag{4}$$

with the Jacobian

$$\mathbf{J} = \frac{\partial \boldsymbol{\psi}}{\partial \boldsymbol{\theta}} \in \mathbb{R}^{D_{\boldsymbol{\psi}} \times D_{\boldsymbol{\theta}}}. \tag{5}$$

The FIM $\boldsymbol{\mathcal{I}}_{\boldsymbol{\psi}} \in \mathbb{R}^{D_{\boldsymbol{\psi}} \times D_{\boldsymbol{\psi}}}$ of the signal model parameters can be computed from the likelihood function $f(\mathbf{r}|\boldsymbol{\psi})$ of the received signal $\mathbf{r}$ conditioned on parameter vector $\boldsymbol{\psi}$,

$$\boldsymbol{\mathcal{I}}_{\boldsymbol{\psi}} = \mathbb{E}_{\mathbf{r}|\boldsymbol{\psi}} \left\{ \left[\frac{\partial}{\partial \boldsymbol{\psi}} \ln f(\mathbf{r}|\boldsymbol{\psi}) \right] \left[\frac{\partial}{\partial \boldsymbol{\psi}} \ln f(\mathbf{r}|\boldsymbol{\psi}) \right]^{\mathrm{T}} \right\}. \tag{6}$$

A. Likelihood Function

The likelihood function $f(\mathbf{r}|\boldsymbol{\psi})$ is defined for the sampled received signal vector $\mathbf{r} = [r(T_{\mathrm{s}}), \ldots, r(NT_{\mathrm{s}})]^{\mathrm{T}} \in \mathbb{C}^N$, containing N samples at rate $1/T_{\mathrm{s}}$. Using the assumption that AWGN and DM are both Gaussian, it is given by

$$\begin{aligned} f(\mathbf{r}|\boldsymbol{\psi}) &\propto \exp\left\{-(\mathbf{r} - \mathbf{S}\boldsymbol{\alpha})^{\mathrm{H}} \mathbf{C}_{\mathrm{n}}^{-1} (\mathbf{r} - \mathbf{S}\boldsymbol{\alpha})\right\} \\ &\propto \exp\left\{2\Re\left\{\mathbf{r}^{\mathrm{H}} \mathbf{C}_{\mathrm{n}}^{-1} \mathbf{S}\boldsymbol{\alpha}\right\} - \boldsymbol{\alpha}^{\mathrm{H}} \mathbf{S}^{\mathrm{H}} \mathbf{C}_{\mathrm{n}}^{-1} \mathbf{S}\boldsymbol{\alpha}\right\} \end{aligned} \tag{7}$$

where $\mathbf{S} = [\mathbf{s}_{\tau_1}, \ldots, \mathbf{s}_{\tau_K}] \in \mathbb{R}^{N \times K}$ is the signal matrix containing delayed versions $\mathbf{s}_{\tau_k} = [s(T_{\mathrm{s}} - \tau_k), s(2T_{\mathrm{s}} - \tau_k), \ldots, s(NT_{\mathrm{s}} - \tau_k)]^{\mathrm{T}}$ of the sampled transmit pulse and $\mathbf{C}_{\mathrm{n}} = \sigma_{\mathrm{n}}^2 \mathbf{I}_N + \mathbf{C}_{\mathrm{c}} \in \mathbb{R}^{N \times N}$ denotes the co-variance matrix of the noise processes. The vector of AWGN samples has variance $\sigma_{\mathrm{n}}^2 = N_0/T_{\mathrm{s}}$; the elements of the DM co-variance matrix are given by $[\mathbf{C}_{\mathrm{c}}]_{n,m} = T_{\mathrm{s}} \sum_{i=1}^{N} S_\nu(iT_{\mathrm{s}}) s(nT_{\mathrm{s}} - iT_{\mathrm{s}}) s(mT_{\mathrm{s}} - iT_{\mathrm{s}})$ (see Appendix A).

This equation can be used to numerically evaluate the likelihood function without further assumptions. It can be evaluated numerically, but the inverse of the covariance matrix $\mathbf{C}_{\mathrm{n}}$, which is needed as a whitening operator to account for the non-stationary DM process, limits the insight it can possibly provide. With the assumption that the received deterministic MPCs $\{\alpha_k s(t - \tau_k)\}$ are orthogonal to one another, i.e. the columns of the signal matrix $\mathbf{S}$ are orthogonal, it can be approximated by

$$\begin{aligned} f(\mathbf{r}|\boldsymbol{\psi}) \propto \exp\Bigg\{ \frac{2}{\sigma_{\mathrm{n}}^2} \Re\left\{ \mathbf{r}^{\mathrm{H}} \sum_{k=1}^{K} w_k^2 \alpha_k \mathbf{s}_{\tau_k} \right\} \\ - \frac{1}{\sigma_{\mathrm{n}}^2} \sum_{k=1}^{K} w_k^2 \left|\alpha_k\right|^2 \mathbf{s}_{\tau_k}^{\mathrm{H}} \mathbf{s}_{\tau_k} \Bigg\} \end{aligned} \tag{8}$$

where $w_k^2 = N_0/(N_0 + T_{\mathrm{N}} S_\nu(\tau_k))$ are whitening weights of the orthogonal pulses, introducing an effective (Nyquist) sampling period T_{N} that corresponds to a block spectrum approximating the pulse $s(t)$. The proof is given in Appendix A. Equation (8) can be interpreted as the sampled version of the continuous likelihood derived in [15]. It shows that the whitening corresponds to a weighting of the MPCs according to the influence of AWGN and diffuse multipath.

B. FIM for the Signal Model Parameters

The FIM $\boldsymbol{\mathcal{I}}_{\boldsymbol{\psi}}$ is obtained from (6) with (7) or (8). Following the notation of [12], it is decomposed according to the subvectors of $\boldsymbol{\psi}$ into

$$\boldsymbol{\mathcal{I}}_{\boldsymbol{\psi}} = \begin{bmatrix} \boldsymbol{\Lambda}_{\mathrm{A}} & \boldsymbol{\Lambda}_{\mathrm{B}}^{\mathrm{R}} & \boldsymbol{\Lambda}_{\mathrm{B}}^{\mathrm{I}} \\ (\boldsymbol{\Lambda}_{\mathrm{B}}^{\mathrm{R}})^{\mathrm{T}} & \boldsymbol{\Lambda}_{\mathrm{C}}' & \mathbf{0} \\ (\boldsymbol{\Lambda}_{\mathrm{B}}^{\mathrm{I}})^{\mathrm{T}} & \mathbf{0} & \boldsymbol{\Lambda}_{\mathrm{C}}' \end{bmatrix} = \begin{bmatrix} \boldsymbol{\Lambda}_{\mathrm{A}} & \boldsymbol{\Lambda}_{\mathrm{B}} \\ \boldsymbol{\Lambda}_{\mathrm{B}}^{\mathrm{T}} & \boldsymbol{\Lambda}_{\mathrm{C}} \end{bmatrix}. \tag{9}$$

Its elements are defined as, for example (see also (D.1)),

$$[\boldsymbol{\Lambda}_{\mathrm{B}}^{\mathrm{R}}]_{k,k'} = \mathbb{E}_{\mathbf{r}|\boldsymbol{\psi}} \left\{ -\frac{\partial^2 \ln f(\mathbf{r}|\boldsymbol{\psi})}{\partial \tau_k \partial \Re\alpha_{k'}} \right\}$$

which yields with (7)

$$\begin{aligned} [\boldsymbol{\Lambda}_{\mathrm{A}}]_{k,k'} &= 2\Re\left\{ \alpha_k \alpha_{k'}^* \left(\frac{\partial \mathbf{s}_{\tau_{k'}}}{\partial \tau_{k'}} \right)^{\mathrm{H}} \mathbf{C}_{\mathbf{n}}^{-1} \frac{\partial \mathbf{s}_{\tau_k}}{\partial \tau_k} \right\} \\ [\boldsymbol{\Lambda}_{\mathrm{B}}^{\mathrm{R}}]_{k,k'} &= 2\Re\left\{ \alpha_k \big(\mathbf{s}_{\tau_{k'}}\big)^{\mathrm{H}} \mathbf{C}_{\mathbf{n}}^{-1} \frac{\partial \mathbf{s}_{\tau_k}}{\partial \tau_k} \right\} \\ [\boldsymbol{\Lambda}_{\mathrm{B}}^{\mathrm{I}}]_{k,k'} &= 2\Im\left\{ \alpha_k \big(\mathbf{s}_{\tau_{k'}}\big)^{\mathrm{H}} \mathbf{C}_{\mathbf{n}}^{-1} \frac{\partial \mathbf{s}_{\tau_k}}{\partial \tau_k} \right\} \\ [\boldsymbol{\Lambda}_{\mathrm{C}}']_{k,k'} &= 2\Re\left\{ \big(\mathbf{s}_{\tau_k}\big)^{\mathrm{H}} \mathbf{C}_{\mathbf{n}}^{-1} \mathbf{s}_{\tau_{k'}} \right\}. \end{aligned}$$

C. Position Error Bound

The FIM $\boldsymbol{\mathcal{I}}_{\boldsymbol{\psi}}$ of the signal model parameters quantifies the information gained from the measurement $\mathbf{r}$ on the signal parameters. The position-related part of this information lies in the MPC delays $\boldsymbol{\tau}$, which are a function of the position $\mathbf{p}$. With appropriate prior knowledge, such as the room geometry, this information can be used beneficially for positioning.

To compute the position error bound (PEB), which represents the CRLB on the position error, we need the upper left 2×2 submatrix of the inverse of FIM $\boldsymbol{\mathcal{I}}_{\boldsymbol{\theta}}$,

$$\mathcal{P}\{\mathbf{p}\} = \sqrt{\mathrm{tr}\left\{ \left[\boldsymbol{\mathcal{I}}_{\boldsymbol{\theta}}^{-1}\right]_{2\times 2} \right\}} = \sqrt{\mathrm{tr}\left\{\boldsymbol{\mathcal{I}}_{\mathbf{p}}^{-1}\right\}}, \tag{10}$$

which can be obtained with (4) and (5) using the blockwise inversion lemma. This results in the so-called *equivalent* FIM (EFIM) $\boldsymbol{\mathcal{I}}_{\mathbf{p}}$ [12],

$$\boldsymbol{\mathcal{I}}_{\mathbf{p}} = \mathbf{H}^{\mathrm{T}} \big(\boldsymbol{\Lambda}_{\mathrm{A}} - \boldsymbol{\Lambda}_{\mathrm{B}} \big(\boldsymbol{\Lambda}_{\mathrm{C}}\big)^{-1} \boldsymbol{\Lambda}_{\mathrm{B}}^{\mathrm{T}}\big) \mathbf{H},$$

which represents the information relevant for the position error bound. Matrix $\mathbf{H} = \partial\boldsymbol{\tau}/\partial\mathbf{p}$ is the submatrix of Jacobian (5) that relates to the position-related information, the derivatives of the delay vector $\boldsymbol{\tau}$ w.r.t. postition $\mathbf{p}$. It describes the variation of the signal parameters w.r.t. the position and can assume different, scenario-dependent forms, depending on the roles of anchors and agents. General expressions for these *spatial delay gradients* are derived in the next section.

IV. Spatial Delay Gradients

The following notations are used to find the elements of matrix $\mathbf{H}$: $\mathbf{p}^{(m)} \in \mathbb{R}^2$ is the position of the m-th agent, where $m \in \mathcal{N}_m = \{1, 2, \ldots, M\}$. $\mathbf{p}_1^{(j)} \in \mathbb{R}^2$ is the position of the j-th fixed anchor, $j \in \mathcal{N}_j = \{M+1, \ldots, M+J\}$, with VAs at positions $\mathbf{p}_k^{(j)} \in \mathbb{R}^2$. In the cooperative scenario, we

replace j with an arbitrary index ξ to cover fixed anchors as well as agents which act as anchors. The corresponding VAs are at $\mathbf{p}_k^{(\xi)} \in \mathbb{R}^2$. To describe gradients w.r.t. anchor or agent position, we use an index η, introducing $\mathbf{p}^{(\eta)} \in \mathbb{R}^2$.

The delay of the k-th MPC is defined by the distance between the k-th VA and the m-th agent,

$$\tau_k^{(\xi,m)} = \frac{1}{c}\left\|\mathbf{p}^{(m)} - \mathbf{p}_k^{(\xi)}\right\| \tag{11}$$

$$= \frac{1}{c}\sqrt{\left(x^{(m)} - x_k^{(\xi)}\right)^2 + \left(y^{(m)} - y_k^{(\xi)}\right)^2}. \tag{12}$$

The angle of vector $(\mathbf{p}^{(m)} - \mathbf{p}_k^{(\xi)})$ is written as $\phi_k^{(\xi,m)}$. To describe the relation between the signal parameter $\tau_k^{(\xi,m)}$ and the geometry, we need to analyze the spatial delay gradient, the derivative of the delay $\tau_k^{(\xi,m)}$ w.r.t. position $\mathbf{p}^{(\eta)}$,

$$\begin{aligned}\mathbf{h}_k^{(\xi,\eta,m)} =& \frac{\partial \tau_k^{(\xi,m)}}{\partial \mathbf{p}^{(\eta)}} = \frac{1}{c}\frac{\partial\left\|\mathbf{p}^{(m)} - \mathbf{p}_k^{(\xi)}\right\|}{\partial \mathbf{p}^{(\eta)}} \\ =& \frac{1}{c}\frac{\partial\left(x^{(m)} - x_k^{(\xi)}\right)}{\partial \mathbf{p}^{(\eta)}}\frac{x^{(m)} - x_k^{(\xi)}}{\left\|\mathbf{p}^{(m)} - \mathbf{p}_k^{(\xi)}\right\|} \\ &+ \frac{1}{c}\frac{\partial\left(y^{(m)} - y_k^{(\xi)}\right)}{\partial \mathbf{p}^{(\eta)}}\frac{y^{(m)} - y_k^{(\xi)}}{\left\|\mathbf{p}^{(m)} - \mathbf{p}_k^{(\xi)}\right\|} \\ =& \frac{1}{c}\left(\delta_{m,\eta}\mathbf{I}_2 - \delta_{\eta,\xi}\frac{\partial \mathbf{p}_k^{(\xi)}}{\partial \mathbf{p}^{(\xi)}}\right)^{\mathrm{T}} \mathbf{e}\left(\phi_k^{(\xi,m)}\right)\end{aligned} \tag{13}$$

where $\mathbf{e}(\phi) := [\cos(\phi), \sin(\phi)]^{\mathrm{T}}$ is a unit vector in direction of the argument angle and $\delta_{m,\eta}$ is the Kronecker delta.

In Appendix B we show that the Jacobian of a VA position w.r.t. its respective anchor's position is given by

$$\left(\frac{\partial \mathbf{p}_k^{(\xi)}}{\partial \mathbf{p}^{(\xi)}}\right)^{\mathrm{T}} = \mathbf{Rot}\left(2\bar{\gamma}_k^{(\xi)}\right)\begin{bmatrix} 1 & 0 \\ 0 & -1 \end{bmatrix}^{Q_k^{(\xi)}} \tag{14}$$

where

$$\mathbf{Rot}(\gamma) := \begin{bmatrix} \cos(\gamma) & -\sin(\gamma) \\ \sin(\gamma) & \cos(\gamma) \end{bmatrix} \tag{15}$$

defines the rotation matrix, $Q_k^{(\xi)}$ is the VA order, i.e. the number of signal reflections of MPC k, and $\bar{\gamma}_k^{(\xi)}$ is the effective wall angle, an alternating sum of wall angles

$$\bar{\gamma}_k^{(\xi)} := \sum_{q=1}^{Q_k^{(\xi)}} (-1)^{q-1}\gamma_{k,q}^{(\xi)} \tag{16}$$

where index q iterates the order of occurence of walls during MPC reflection or VA construction. Using (14) in (13), we get

$$\begin{aligned}&\mathbf{h}_k^{(\xi,\eta,m)} = \\ &\frac{1}{c}\left(\delta_{m,\eta}\mathbf{e}\left(\phi_k^{(\xi,m)}\right) - \delta_{\eta,\xi}\mathbf{e}\left((-1)^{Q_k^{(\xi)}}\phi_k^{(\xi,m)} + 2\bar{\gamma}_k^{(\xi)}\right)\right),\end{aligned} \tag{17}$$

where the first summand represents the influence of the agent position while the second summand is linked to the anchor position. We stack the transposed gradient vectors (17) for the entire set of multipath components in the gradient matrix $\mathbf{H}^{(\xi,\eta,m)} \in \mathbb{R}^{K^{(\xi,m)}\times 2}$ and the matrices for all the agents' derivatives into matrix $\mathbf{H}^{(\xi,m)} \in \mathbb{R}^{K^{(\xi,m)}\times 2M}$.

The following specializations will be used:

1) Bistatic scenario: $k = 1, \ldots, K^{(\xi,m)}$

a) The gradient with respect to the agent: This case describes the derivatives of delay $\tau^{(\xi,m)}$ w.r.t. the agent position, i.e. $\eta = m$, yielding the gradient

$$\mathbf{h}_k^{(\xi,m,m)} = \frac{\partial \tau^{(\xi,m)}}{\partial \mathbf{p}^{(m)}} = \frac{1}{c}\mathbf{e}\left(\phi_k^{(\xi,m)}\right) \tag{18}$$

in direction of the line connecting the two nodes. We define the gradient matrix $\mathbf{H}_{\mathrm{Ag}}^{(\xi,m)} = \mathbf{H}^{(\xi,m,m)} \in \mathbb{R}^{K^{(\xi,m)}\times 2}$.

b) The gradient with respect to the anchor: In this case, the derivatives w.r.t. the anchor position $\mathbf{p}^{(\xi)} = \mathbf{p}_1^{(\xi)}$ are described, i.e. $\eta = \xi$, yielding for the k-th MPC

$$\begin{aligned}\mathbf{h}_k^{(\xi,\xi,m)} &= \frac{\partial \tau_k^{(\xi,m)}}{\partial \mathbf{p}^{(\xi)}} \\ &= -\frac{1}{c}\mathbf{e}\left((-1)^{Q_k^{(\xi)}}\phi_k^{(\xi,m)} + 2\bar{\gamma}_k^{(\xi)}\right) = \frac{1}{c}\mathbf{e}\left(\phi_k^{(m,\xi)}\right)\end{aligned} \tag{19}$$

again in direction of the line connecting the two nodes. The proof for the final equality can be obtained graphically. The gradient matrix is $\mathbf{H}_{\mathrm{An}}^{(\xi,m)} = \mathbf{H}_{\mathrm{Ag}}^{(m,\xi)} = \mathbf{H}^{(\xi,\xi,m)} \in \mathbb{R}^{K^{(\xi,m)}\times 2}$.

2) Monostatic scenario: Here we restrict the VA set to $k = 2, \ldots, K^{(m,m)}$, the agent is as well the anchor, $\xi = m$, and both move synchronously, $\eta = m$, i.e., the two terms in (17) interact with each other. The gradient

$$\begin{aligned}&\mathbf{h}_k^{(m,m,m)} = \frac{\partial \tau_k^{(m,m)}}{\partial \mathbf{p}^{(m)}} \\ &= \frac{1}{c}\left(\mathbf{e}\left(\phi_k^{(m,m)}\right) - \mathbf{e}\left((-1)^{Q_k^{(m)}}\phi_k^{(m,m)} + 2\bar{\gamma}_k^{(m)}\right)\right) \\ &= \begin{cases} \frac{2}{c}\sin\left(\bar{\gamma}_k^{(m)}\right)\mathbf{e}\left(\phi_k^{(m,m)} + \bar{\gamma}_k^{(m)} - \frac{\pi}{2}\right) & \text{If } Q_k^{(m)} \text{is even} \\ \frac{2}{c}\sin\left(\bar{\gamma}_k^{(m)} - \phi_k^{(m,m)}\right)\mathbf{e}\left(\bar{\gamma}_k^{(m)} - \frac{\pi}{2}\right) & \text{If } Q_k^{(m)} \text{is odd} \end{cases}\end{aligned} \tag{20}$$

has been decomposed—as shown in Appendix C—into a magnitude term $0 \leq \left\|\mathbf{h}_k^{(m,m,m)}\right\| \leq \frac{2}{c}$ and a resulting direction vector. Both depend on the angle $\phi_k^{(m,m)}$ itself, the VA order, and the angles of all contributing walls comprised in $\bar{\gamma}_k^{(m)}$. The gradient matrix is $\mathbf{H}_{\mathrm{Mo}}^{(m)} = \mathbf{H}^{(m,m,m)} \in \mathbb{R}^{(K^{(m,m)}-1)\times 2}$.

Single reflections ($Q_k^{(m)} = 1$, $\bar{\gamma}_k^{(m)} = \phi_k^{(m,m)} \pm \frac{\pi}{2}$) and reflections on rectangular corners ($Q_k^{(m)} = 2$, $\bar{\gamma}_k^{(m)} = \pm\frac{\pi}{2}$) constitute important types of monostatic VAs. Both have $\partial\tau_k^{(m,m)}/\partial\mathbf{p}^{(m)} = \frac{2}{c}\mathbf{e}(\phi_k^{(m,m)})$, which is twice as much spatial sensitivity of delays as in the bistatic cases (18) and (19), thus providing higher ranging information. The simplest case of a vanishing gradient (magnitude zero) is a second-order reflection between parallel walls ($Q_k^{(m)} = 2$, $\bar{\gamma}_k^{(m)} = 0$).

V. CRLB on the Position Error

In this Section, the CRLB on the position error is derived for ToA, TDoA, and a cooperative scenario. In the latter, the agents execute radar-type (monostatic) measurements, cooperative (bistatic) measurements to other agents, and also ToA measurements to fixed (physical) anchors.

Using a stack vector $\mathbf{\Psi} = [\mathbf{T}^{\mathrm{T}}, \Re\mathbf{A}^{\mathrm{T}}, \Im\mathbf{A}^{\mathrm{T}}]^{\mathrm{T}}$ of the signal parameters for all relevant nodes, with $\mathbf{T}$ combining the delays

and $\mathbf{A}$ combining the amplitudes, the Jacobian (5) has the following general structure for any measurement scenario.

$$\mathbf{J} = \frac{\partial \boldsymbol{\Psi}}{\partial \boldsymbol{\Theta}} = \begin{bmatrix} \mathbf{H} & \mathbf{L} & \mathbf{0} \\ \mathbf{0} & \mathbf{0} & \mathbf{I} \end{bmatrix} \tag{21}$$
$$= \begin{bmatrix} \partial\mathbf{T}/\partial\mathbf{P} & \partial\mathbf{T}/\partial\boldsymbol{\epsilon} & \partial\mathbf{T}/\partial\Re\mathbf{A} & \partial\mathbf{T}/\partial\Im\mathbf{A} \\ \partial\Re\mathbf{A}/\partial\mathbf{P} & \partial\Re\mathbf{A}/\partial\boldsymbol{\epsilon} & \partial\Re\mathbf{A}/\partial\Re\mathbf{A} & \partial\Re\mathbf{A}/\partial\Im\mathbf{A} \\ \partial\Im\mathbf{A}/\partial\mathbf{P} & \partial\Im\mathbf{A}/\partial\boldsymbol{\epsilon} & \partial\Im\mathbf{A}/\partial\Re\mathbf{A} & \partial\Im\mathbf{A}/\partial\Im\mathbf{A} \end{bmatrix}$$

Vector $\boldsymbol{\Theta} = [\mathbf{P}^{\mathrm{T}}, \boldsymbol{\epsilon}^{\mathrm{T}}, \Re\mathbf{A}^{\mathrm{T}}, \Im\mathbf{A}^{\mathrm{T}}]^{\mathrm{T}}$, spatial delay gradient $\mathbf{H} = \partial\mathbf{T}/\partial\mathbf{P}$, and gradient $\mathbf{L} = \partial\mathbf{T}/\partial\boldsymbol{\epsilon}$ are specifically defined in the following three subsections for different cases.

A. Derivation of the CRLB for Multipath-ToA

Due to the fact that for ToA and TDoA only one agent is present, we drop the agent index m so that $\mathbf{P} = \mathbf{p}$, and define $\mathcal{N}_j = \{1, 2, \ldots, J\}$. For the ToA approach we can use the geometry for the bistatic scenario, case (a). The clock-offset $\boldsymbol{\epsilon}$ is considered to be known and zero. Due to the assumption that the measurements $\mathbf{r}^{(j)}$ from all J anchors are independent, the log-likelihood function is defined as

$$\ln f(\mathbf{R}|\boldsymbol{\Psi}) = \sum_{j\in\mathcal{N}_j} \ln f\big(\mathbf{r}^{(j)}|\boldsymbol{\tau}^{(j)}, \boldsymbol{\alpha}^{(j)}\big), \tag{22}$$

where $\mathbf{R} = \big[\big(\mathbf{r}^{(1)}\big)^{\mathrm{T}}, \ldots, \big(\mathbf{r}^{(J)}\big)^{\mathrm{T}}\big]^{\mathrm{T}}$ combines all measurements and $\boldsymbol{\tau}^{(j)}$ and $\boldsymbol{\alpha}^{(j)}$ are the delay and amplitude vectors respectively, corresponding to measurement $\mathbf{r}^{(j)}$. The Jacobian $\mathbf{J}$ has the following structure,

$$\mathbf{J} = \begin{bmatrix} \mathbf{H}^{(1)}_{K^{(1)}\times 2} & & \\ \vdots & & \\ \mathbf{H}^{(J)}_{K^{(J)}\times 2} & & \\ & & \mathbf{I}_{D_{\mathbf{I}}\times D_{\mathbf{I}}} \end{bmatrix}, \tag{23}$$

where zero-matrices in the off-diagonal blocks are skipped for clarity and $D_{\mathbf{I}} = 2\sum_{j=1}^{J} K^{(j)}$. The subblocks $\mathbf{H}^{(j)} = \mathbf{H}^{(j,1)}_{\mathrm{Ag}}$ account for the geometry as described in Section IV. Due to the independence of the received signals, the EFIMs $\boldsymbol{\mathcal{I}}^{(j)}_{\mathbf{p}}$ from the J different anchors are additive. Using Equation (4) and the block structure of $\boldsymbol{\mathcal{I}}^{(j)}_{\boldsymbol{\psi}}$, we can write the EFIM as a canonical sum

$$\boldsymbol{\mathcal{I}}_{\mathbf{p}} = \sum_{j\in\mathcal{N}_j} \big(\mathbf{H}^{(j)}\big)^{\mathrm{T}} \Big(\boldsymbol{\Lambda}^{(j)}_{\mathrm{A}} - \boldsymbol{\Lambda}^{(j)}_{\mathrm{B}} \big(\boldsymbol{\Lambda}^{(j)}_{\mathrm{C}}\big)^{-1} \big(\boldsymbol{\Lambda}^{(j)}_{\mathrm{B}}\big)^{\mathrm{T}}\Big) \mathbf{H}^{(j)} \tag{24}$$

where $\boldsymbol{\Lambda}^{(j)}_{\mathrm{A}}$, $\boldsymbol{\Lambda}^{(j)}_{\mathrm{B}}$, and $\boldsymbol{\Lambda}^{(j)}_{\mathrm{C}}$ are subblocks of $\boldsymbol{\mathcal{I}}^{(j)}_{\boldsymbol{\psi}}$ defined in (9). Expression (24) simplifies when we assume no path overlap (i.e. orthogonality) between signals from different VAs. In this case, $\boldsymbol{\Lambda}_{\mathrm{B}} = \mathbf{0}$ and $\boldsymbol{\Lambda}_{\mathrm{A}}$ will be diagonal. Using the result of Appendix D we can then write

$$\begin{aligned} \boldsymbol{\mathcal{I}}_{\mathbf{p}} &= \sum_{j\in\mathcal{N}_j} \big(\mathbf{H}^{(j)}\big)^{\mathrm{T}} \boldsymbol{\Lambda}^{(j)}_{\mathrm{A}} \mathbf{H}^{(j)} \\ &\approx \frac{8\pi^2\beta^2}{c^2} \sum_{j\in\mathcal{N}_j} \sum_{k=1}^{K^{(j)}} \mathrm{SINR}^{(j)}_k \mathbf{D}_{\mathrm{r}}(\phi^{(j)}_k) \end{aligned} \tag{25}$$

where β is the effective (mean square) bandwidth of $s(t)$ (see Appendix D),

$$\mathrm{SINR}^{(j)}_k := \big(w^{(j)}_k\big)^2 \frac{\big|\alpha^{(j)}_k\big|^2}{N_0} = \frac{\big|\alpha^{(j)}_k\big|^2}{N_0 + T_{\mathrm{N}} S^{(j)}_{\nu}\big(\tau^{(j)}_k\big)} \tag{26}$$

is the signal-to-interference-plus-noise ratio (SINR) of the k-th MPC of the j-th anchor, and

$$\mathbf{D}_{\mathrm{r}}(\phi^{(j)}_k) = \mathbf{e}(\phi^{(j)}_k)\mathbf{e}(\phi^{(j)}_k)^{\mathrm{T}} \tag{27}$$

is called ranging direction matrix (cf. [12]), a rank-one matrix with an eigenvector in direction of $\phi^{(j)}_k$.

Valuable insight is gained from (25) and (26). In particular,

- Each VA (i.e. each deterministic MPC) adds some positive term to the EFIM in direction of $\phi^{(j)}_k$ and hence reduces the PEB in direction of $\phi^{(j)}_k$.
- The $\mathrm{SINR}^{(j)}_k$ determines the magnitude of this contribution (cf. ranging intensity information (RII) in [12]). It is limited by diffuse multipath as quantified by coefficient $w^{(j)}_k$, an effect that scales with effective pulse duration T_{N} (cf. (26)) and thus inversly with the bandwidth.
- The effective bandwidth β scales the EFIM. Any increase corresponds to a decreased PEB.

Discussion of *path overlap* (cf. [12]):

- $\tau_k - \tau_{k'} \ll T_{\mathrm{N}}$: In this case the MPCs can not be distinguished and the position-related information is entirely lost.
- $\tau_k - \tau_{k'} \approx T_{\mathrm{N}}$: In this case the MPCs are correlated, but the position-related information can still partly be used. The discrete-time formulation of the CRLB based on (7) can quantify this information gain appropriately, in contrast to our previous, continuous formulation in [15].
- $\tau_k - \tau_{k'} \gg T_{\mathrm{N}}$: In this case, MPCs are considered to be orthogonal and (25) can be used if it holds for all $k \neq k'$.

B. Derivation of the CRLB for Multipath-TDoA

Next we consider the same setup as before, but assume the clock offsets $\boldsymbol{\epsilon}$ to be unknown parameters. The differences between arrival times still provide position information in this case, hence it has been named TDoA.

When using multiple anchors, we distinguish two different scenarios where either the clocks of all anchors are synchronized among each other, or alternatively no synchronization is present at all. While this does not affect the signal parameter FIM, we need to take it into account when performing the parameter transformation. Apart from the partial derivatives $\mathbf{L} = \partial\mathbf{T}/\partial\boldsymbol{\epsilon}$, the terms of the Jacobian are identical for ToA and TDoA, resulting in

$$\mathbf{J} = \begin{bmatrix} \mathbf{H}^{(1)}_{K^{(1)}\times 2} & \mathbf{L}^{(1)}_{K^{(1)}\times D_{\boldsymbol{\epsilon}}} & \\ \vdots & \vdots & \\ \mathbf{H}^{(J)}_{K^{(J)}\times 2} & \mathbf{L}^{(J)}_{K^{(J)}\times D_{\boldsymbol{\epsilon}}} & \\ & & \mathbf{I}_{D_{\mathbf{I}}\times D_{\mathbf{I}}} \end{bmatrix}, \tag{28}$$

where $\mathbf{L}^{(j)} = \partial\boldsymbol{\tau}^{(j)}/\partial\boldsymbol{\epsilon}$ and $D_{\boldsymbol{\epsilon}}$ is the length of $\boldsymbol{\epsilon}$.

Synchronized anchors: When assuming $\epsilon^{(1)} = \cdots = \epsilon^{(J)} = \epsilon$, the vector $\boldsymbol{\epsilon}$ reduces to $\boldsymbol{\epsilon} = \epsilon$. The derivatives

of the arrival times with respect to the clock offset are then given by $\mathbf{L}^{(j)} = \mathbf{l}_{\text{syn}}^{(j)} = [1, \ldots, 1]^{\mathrm{T}}$. Applying the parameter transformation and computing the block inverse similar as in (24) leads to additivity of the 3×3 EFIMs $\boldsymbol{\mathcal{I}}_{\mathbf{p},\epsilon}^{(j)}$ for the extended parameter vector $[\mathbf{p}^{\mathrm{T}}, \epsilon]^{\mathrm{T}}$ (see Appendix E). When neglecting path overlap this expression simplifies to

$$\boldsymbol{\mathcal{I}}_{\mathbf{p},\epsilon} = \sum_{j\in\mathcal{N}_j} \boldsymbol{\mathcal{I}}_{\mathbf{p},\epsilon}^{(j)} = 8\pi^2\beta^2 \sum_{j\in\mathcal{N}_j} \sum_{k=1}^{K^{(j)}} \mathrm{SINR}_k^{(j)} \mathbf{D}_{\mathrm{r},\epsilon}(\phi_k^{(j)}), \tag{29}$$

with

$$\mathbf{D}_{\mathrm{r},\epsilon}(\phi_k^{(j)}) = \mathbf{v}\mathbf{v}^{\mathrm{T}},\ \mathbf{v} = \left[\frac{1}{c}\cos(\phi_k^{(j)}),\ \frac{1}{c}\sin(\phi_k^{(j)}),\ 1\right]^{\mathrm{T}}.$$

The inner sum in (29) reveals that the 3×3 EFIMs $\boldsymbol{\mathcal{I}}_{\mathbf{p},\epsilon}^{(j)}$ are in canonical form. Since $\mathbf{D}_{r,\epsilon}$ is a positive semidefinite matrix, it highlights that each VA adds information for the estimation of $\mathbf{p}$ and ϵ, scaled by its SINR and β.

The EFIM $\boldsymbol{\mathcal{I}}_{\mathbf{p}}$ can be computed from $\boldsymbol{\mathcal{I}}_{\mathbf{p},\epsilon}$ by again applying the blockwise inversion lemma. When neglecting path overlap, the expression for $\boldsymbol{\mathcal{I}}_{\mathbf{p}}$ simplifies to

$$\boldsymbol{\mathcal{I}}_{\mathbf{p}} = \frac{8\pi^2\beta^2}{c^2}\left[\sum_{j\in\mathcal{N}_j}\sum_{k=1}^{K^{(j)}} \mathrm{SINR}_k^{(j)} \mathbf{D}_{\mathrm{r}}(\phi_k^{(j)}) - \boldsymbol{\mathcal{C}}\right], \tag{30}$$

where $\boldsymbol{\mathcal{C}}$ accounts for the (negative) influence of the clock offset estimation with

$$\boldsymbol{\mathcal{C}} = \frac{1}{\sum_{j\in\mathcal{N}_j}\sum_{k=1}^{K^{(j)}} \mathrm{SINR}_k^{(j)}} \mathbf{c}\mathbf{c}^{\mathrm{T}},$$
$$\mathbf{c} = \sum_{j\in\mathcal{N}_j}\sum_{k=1}^{K^{(j)}} \mathrm{SINR}_k^{(j)} \mathbf{e}(\phi_k^{(j)}).$$

Note that TDoA can theoretically achieve equal performance as ToA under the rather unlikely condition $\mathbf{c} = \mathbf{0}$. Otherwise $\boldsymbol{\mathcal{C}}$ reduces the information, and thereby increases the PEB with respect to ToA.

Asynchronous anchors: When having $\epsilon^{(i)} \neq \epsilon^{(j)}$, $\forall i \neq j$, $i, j \in \mathcal{N}_j$, we stack all clock offsets in the vector $\boldsymbol{\epsilon} = [\epsilon^{(1)}, \ldots, \epsilon^{(J)}]^{\mathrm{T}}$. The derivatives of the arrival times with respect to the clock offsets are then given by a gradient matrix $\mathbf{L} = \partial\mathbf{T}/\partial\boldsymbol{\epsilon}$ of size $\sum_{j\in\mathcal{N}_j} K^{(j)} \times J$ which stacks submatrices $\mathbf{L}_{\text{asyn}}^{(j)}$ with one nonzero column $[\mathbf{L}_{\text{asyn}}^{(j)}]_{i,j} = 1,\ i = 1, \ldots, K^{(j)}$. This leads to the additivity of the 2×2 EFIM for TDoA as shown in Appendix E, i.e. $\boldsymbol{\mathcal{I}}_{\mathbf{p}} = \sum_{j\in\mathcal{N}_j} \boldsymbol{\mathcal{I}}_{\mathbf{p}}^{(j)}$. When neglecting path overlap, $\boldsymbol{\mathcal{I}}_{\mathbf{p}}$ takes the form of (30), but with

$$\boldsymbol{\mathcal{C}} = \sum_{j\in\mathcal{N}_j} \frac{1}{\sum_{k=1}^{K^{(j)}} \mathrm{SINR}_k^{(j)}} \mathbf{c}^{(j)} \left(\mathbf{c}^{(j)}\right)^{\mathrm{T}}, \tag{31}$$

$$\mathbf{c}^{(j)} = \sum_{k=1}^{K^{(j)}} \mathrm{SINR}_k^{(j)} \mathbf{e}(\phi_k^{(j)}).$$

Again, equality with ToA is obtained if each $\mathbf{c}^{(j)} = \mathbf{0}$, otherwise the PEB is increased.

C. Derivation of the CRLB for Multipath-Coop

We assume M agents $m \in \mathcal{N}_m = \{1, 2, \ldots, M\}$ and J fixed anchors $j \in \mathcal{N}_j = \{M+1, \ldots, M+J\}$, which cooperate with one another. As outlined in the Introduction, every agent conducts a monostatic measurement, meaning it emits a pulse and receives the multipath signal reflected by the environment, and conventional bistatic measurements with all other agents and the fixed anchors. All measurements are distributed such that every agent is able to exploit information from any of its received and/or transmitted signals. The clock-offsets $\boldsymbol{\epsilon}$ are considered to be zero.

The signal parameter vectors for the (j, m)-th received signal $\mathbf{r}^{(j,m)}$ are defined as $\boldsymbol{\tau}^{(j,m)} = \left[\tau_1^{(j,m)}, \ldots, \tau_{K^{(j,m)}}^{(j,m)}\right]^{\mathrm{T}}$ and $\boldsymbol{\alpha}^{(j,m)} = \left[\alpha_1^{(j,m)}, \ldots, \alpha_{K^{(j,m)}}^{(j,m)}\right]^{\mathrm{T}}$. For deriving the cooperative EFIM, we stack positions $\mathbf{p}^{(m)}$ of the M agents into the vector

$$\mathbf{P} = \left[\left(\mathbf{p}^{(1)}\right)^{\mathrm{T}}, \ldots, \left(\mathbf{p}^{(M)}\right)^{\mathrm{T}}\right]^{\mathrm{T}} \in \mathbb{R}^{2M\times1} \tag{32}$$

and all measurements $\mathbf{r}^{(j,m)}$ in the vector

$$\mathbf{R} = \left[\left(\mathbf{r}^{(1,1)}\right)^{\mathrm{T}}, \ldots, \left(\mathbf{r}^{(1,M)}\right)^{\mathrm{T}}, \ldots, \left(\mathbf{r}^{(M,M)}\right)^{\mathrm{T}}, \left(\mathbf{r}^{(M+1,1)}\right)^{\mathrm{T}}, \ldots, \left(\mathbf{r}^{(M+J,M)}\right)^{\mathrm{T}}\right]^{\mathrm{T}} \in \mathbb{C}^{D_{\mathbf{R}}\times1}, \tag{33}$$

where $D_{\mathbf{R}} = NM(M + J)$. Further, we stack the signal parameters correspondingly in the vectors

$$\mathbf{T} = \left[\left(\boldsymbol{\tau}^{(1,1)}\right)^{\mathrm{T}}, \ldots, \left(\boldsymbol{\tau}^{(1,M)}\right)^{\mathrm{T}}, \ldots, \left(\boldsymbol{\tau}^{(M+J,M)}\right)^{\mathrm{T}}\right]^{\mathrm{T}} \tag{34}$$

and

$$\mathbf{A} = \left[\left(\boldsymbol{\alpha}^{(1,1)}\right)^{\mathrm{T}}, \ldots, \left(\boldsymbol{\alpha}^{(1,M)}\right)^{\mathrm{T}}, \ldots, \left(\boldsymbol{\alpha}^{(M+J,M)}\right)^{\mathrm{T}}\right]^{\mathrm{T}} \tag{35}$$

of length $D_{\mathbf{T}} = D_{\mathbf{A}} = \sum_{j\in(\mathcal{N}_m\cup\mathcal{N}_j)} \sum_{m\in\mathcal{N}_m} K^{(j,m)}$ to construct vector $\boldsymbol{\Psi} = [\mathbf{T}^{\mathrm{T}}, \Re\mathbf{A}^{\mathrm{T}}, \Im\mathbf{A}^{\mathrm{T}}]^{\mathrm{T}}$. The corresponding joint log-likelihood function, assuming independent measurements $\mathbf{r}^{(j,m)}$ between the cooperating nodes, is defined as

$$\ln f(\mathbf{R}|\boldsymbol{\Psi}) = \sum_{j\in(\mathcal{N}_m\cup\mathcal{N}_j)} \sum_{m\in\mathcal{N}_m} \ln f\left(\mathbf{r}^{(j,m)}|\boldsymbol{\tau}^{(j,m)}, \boldsymbol{\alpha}^{(j,m)}\right). \tag{36}$$

The EFIM $\boldsymbol{\mathcal{I}}_{\mathbf{P}}$ is described by (see Appendix F)

$$\boldsymbol{\mathcal{I}}_{\mathbf{P}} = \sum_{j\in(\mathcal{N}_m\cup\mathcal{N}_j)} \sum_{m\in\mathcal{N}_m} \left(\mathbf{H}^{(j,m)}\right)^{\mathrm{T}} \boldsymbol{\Lambda}^{(j,m)} \mathbf{H}^{(j,m)} \tag{37}$$

where

$$\boldsymbol{\Lambda}^{(j,m)} = \boldsymbol{\Lambda}_{\mathrm{A}}^{(j,m)} - \boldsymbol{\Lambda}_{\mathrm{B}}^{(j,m)} \left(\boldsymbol{\Lambda}_{\mathrm{C}}^{(j,m)}\right)^{-1} \left(\boldsymbol{\Lambda}_{\mathrm{B}}^{(j,m)}\right)^{\mathrm{T}} \tag{38}$$

yields the sub-blocks $\boldsymbol{\mathcal{I}}_{\boldsymbol{\psi}}^{(j,m)}$ of the FIM for the likelihood function (36), for independent measurements, and $\mathbf{H}^{(j,m)}$ are the spatial delay gradients of the Jacobian

$$\mathbf{J} = \begin{bmatrix} \mathbf{H}_{K^{(1,1)}\times2M}^{(1,1)} \\ \vdots \\ \mathbf{H}_{K^{(1,M)}\times2M}^{(1,M)} \\ \vdots \\ \mathbf{H}_{K^{(M+J,M)}\times2M}^{(M+J,M)} & \mathbf{I}_{D_{\mathbf{I}}\times D_{\mathbf{I}}} \end{bmatrix}, \tag{39}$$

TABLE I
CHANNEL PARAMETERS FOR NUMERICAL EVALUATIONS.

	Parameter	Value	Description
Deterministic MPCs		2 3 dB	max. VA order attenuation per reflection
Signal parameters	f_c T_p β_{R}	7 GHz 1 ns, (0.5 ns,2 ns) RRC 0.6	carrier frequency pulse duration pulse shape roll-off factor
PDP of diffuse multipath	Ω_1 γ_1 γ_{rise} χ	$1.16 \cdot 10^{-6}$ 20 ns 5 ns 0.98	normalized power shape parameters
AWGN	$N_0/2$	10^{-8}	PSD

where $D_{\mathbf{I}} = 2D_{\mathbf{A}}$.[2] As shown in Appendix F, one gets the following final result for the EFIM $\boldsymbol{\mathcal{I}}_{\mathbf{p}}$ for all agents

$$\boldsymbol{\mathcal{I}}_{\mathbf{P}} = \begin{bmatrix} \boldsymbol{\mathcal{I}}_{\mathrm{Mo}}^{(1)} + 2\boldsymbol{\mathcal{I}}_{\mathrm{Ag}}^{(1)} + \boldsymbol{\mathcal{I}}_{\mathrm{An}}^{(1)} & 2\boldsymbol{\mathcal{I}}_{\mathrm{C}}^{(1,2)} & \dots & 2\boldsymbol{\mathcal{I}}_{\mathrm{C}}^{(1,M)} \\ 2\boldsymbol{\mathcal{I}}_{\mathrm{C}}^{(2,1)} & \ddots & & \\ \vdots & & & \\ 2\boldsymbol{\mathcal{I}}_{\mathrm{C}}^{(M,1)} & & \boldsymbol{\mathcal{I}}_{\mathrm{Mo}}^{(M)} + 2\boldsymbol{\mathcal{I}}_{\mathrm{Ag}}^{(M)} + \boldsymbol{\mathcal{I}}_{\mathrm{An}}^{(M)} \end{bmatrix}. \tag{40}$$

The diagonal blocks $\boldsymbol{\mathcal{I}}_{\mathrm{Ag}}^{(\eta)} = \sum_{m \in \mathcal{N}_m \setminus \{\eta\}} \left(\mathbf{H}_{\mathrm{Ag}}^{(m,\eta)}\right)^{\mathrm{T}} \boldsymbol{\Lambda}^{(m,\eta)} \mathbf{H}_{\mathrm{Ag}}^{(m,\eta)}$ account for the bistatic measurements between agent η and all other agents, $\boldsymbol{\mathcal{I}}_{\mathrm{An}}^{(\eta)} = \sum_{j \in \mathcal{N}_j} \left(\mathbf{H}_{\mathrm{Ag}}^{(j,\eta)}\right)^{\mathrm{T}} \boldsymbol{\Lambda}^{(j,\eta)} \mathbf{H}_{\mathrm{Ag}}^{(j,\eta)}$ account for the bistatic measurements between agent η and all fixed anchors, and $\boldsymbol{\mathcal{I}}_{\mathrm{Mo}}^{(\eta)} = \left(\mathbf{H}_{\mathrm{Mo}}^{(\eta)}\right)^{\mathrm{T}} \boldsymbol{\Lambda}^{(\eta,\eta)} \mathbf{H}_{\mathrm{Mo}}^{(\eta)}$ account for the monostatic measurement of agent η. The off-diagonal blocks $\boldsymbol{\mathcal{I}}_{\mathrm{C}}^{(\eta,\eta')} = \left(\mathbf{H}_{\mathrm{Ag}}^{(\eta',\eta)}\right)^{\mathrm{T}} \boldsymbol{\Lambda}^{(\eta',\eta)} \mathbf{H}_{\mathrm{Ag}}^{(\eta,\eta')}$ account for the uncertainty about the cooperating agents in their role as anchors (cf. (F.3) and (F.4)). This has a negative effect on the localization performance of the agents. The factors of two in (40), related to the EFIM of measurements in-between agents, results from the fact that those measurements are performed twice. This simplifies the notations in this section. If such repeated measurements are avoided, the same result would apply but with these factors removed.

Finally, the CRLB on position $\mathbf{p}^{(\eta)}$ of agent η is

$$\mathcal{P}\{\mathbf{p}^{(\eta)}\} = \sqrt{\mathrm{tr}\left\{\left[\boldsymbol{\mathcal{I}}_{\mathbf{P}}^{-1}\right]_{2\times 2}^{(\eta,\eta)}\right\}}. \tag{41}$$

VI. RESULTS

The computational results are shown for a room illustrated in Fig. 2. For the ToA and TDoA scenarios, we assume one or two fixed anchors at $\mathbf{p}_1^{(1)} = [10, 7]^{\mathrm{T}}$ and $\mathbf{p}_1^{(2)} = [2, 1]^{\mathrm{T}}$ and one moving agent at an arbitrary position. For the cooperative scenario, the two anchors act as cooperating agents with fixed (but unknown) positions, such that in total 3 agents cooperate. For all three setups, VAs up to order two are considered. For all evaluations of the PEB, we use a point grid with a resolution of 2 cm, resulting in 180,000 points covering the entire room.

As transmit signal $s(t)$, we use a root-raised-cosine (RRC) pulse with unit energy and a roll-off factor $\beta_{\mathrm{R}} = 0.6$, modulated on a carrier frequency of $f_c = 7\,\mathrm{GHz}$. The computations are done for pulse durations of $T_{\mathrm{p}} = 0.5\,\mathrm{ns}$, $T_{\mathrm{p}} = 1\,\mathrm{ns}$ and $T_{\mathrm{p}} = 2\,\mathrm{ns}$. For all antennas, we assume isotropic antenna patterns in the azimuth domain and matching polarizations. The free-space pathloss is modeled by the Friis equation. To account for the material impact, we assume 3 dB attenuation per reflection. The PDP of the DM is considered to be a fixed double-exponential function, cf. [21, eq. (9)]. This choice has also been made in [15] as it reflects the common assumption of an exponential decay of the DM power and also accounts for the fact that the LOS component is not impaired by DM as severely as MPCs arriving later. All channel-specific parameters for the deterministic MPCs, DM and AWGN are summarized in Table I.

A. Multipath-ToA

Fig. 2 shows the PEB over the floor-plan of the room for ToA and $T_{\mathrm{p}} = 1\,\mathrm{ns}$. Fig. 2(a) indicates that the PEB neglecting path-overlap (cf. (25), where $T_{\mathrm{N}} = T_{\mathrm{p}}$ for an RRC pulse) is below 10 cm for most of the area for just one physical anchor at position $\mathbf{p}_1^{(1)}$. The entire room is covered even though the anchor is partly not visible at the agent positions. One can clearly see the visibility regions of different VA-modeled MPCs encoded by the level of the PEB. If path-overlap is considered in the computation of the CRLB (using (24)), the adverse effect of room symmetries is observable, corresponding to regions where deterministic MPCs overlap, see Fig. 2(b). In case of *unresolvable* path overlap, i.e. the delay difference of two MPCs is less than the pulse duration $\tau_k - \tau_{k'} \ll T_{\mathrm{p}}$, the information of the corresponding components is entirely lost (see Section V-A). Fig. 2 also shows error ellipses for several positions computed from (10). These ellipses represent the geometrically decomposed PEB with twenty-fold error standard-deviation. Fig. 2(c) shows the PEB for the same parameters but for two anchors at $\mathbf{p}_1^{(1)}$ and $\mathbf{p}_1^{(2)}$, considering path-overlap. The error ellipses clearly indicate that the PEB is much smaller and the impact of path overlap has been reduced.

A quantitative assessment for the scenarios in Fig. 2 is given in Figs. 3 and 4, which show the CDFs of the PEB for different pulse durations ($T_{\mathrm{p}} = 0.5\,\mathrm{ns}$, $T_{\mathrm{p}} = 1\,\mathrm{ns}$ and $T_{\mathrm{p}} = 2\,\mathrm{ns}$). One can observe that the position error increases vastly w.r.t. this parameter. The "no PO" results account for the proportional scaling of Fisher information with bandwith and additionally for the increased interference power due to DM, both of which are clearly seen in aproximation (25). The influence of path overlap, which is neglected in (25), magnifies this effect even further because its occurrence becomes more probable. Over all, the error magnitude scales by a factor of almost ten, while the pulse duration is scaled by a factor of four. The detrimental effect of path overlap diminishes at $T_{\mathrm{p}} = 0.5\,\mathrm{ns}$.

Our work in [22]–[24] shows algorithms based on the presented signal model that can closely approach these bounds. I.e. cm-level accuracy is obtained for 90 % of the estimates.

[2] Assuming no path overlap, (37) can be simplified as in (25), using the result from Appendix D.

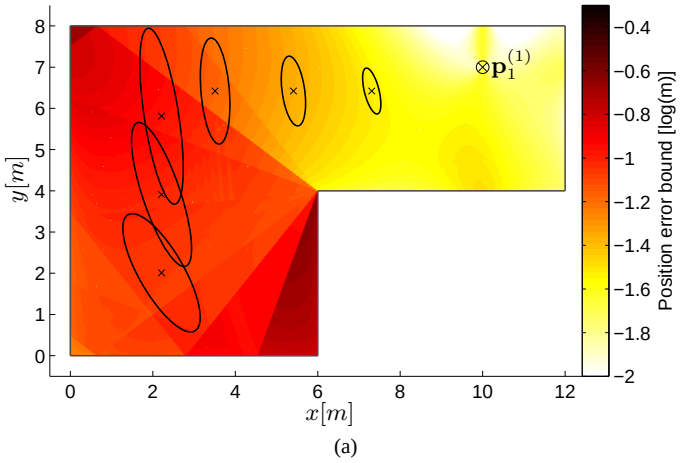

(a)

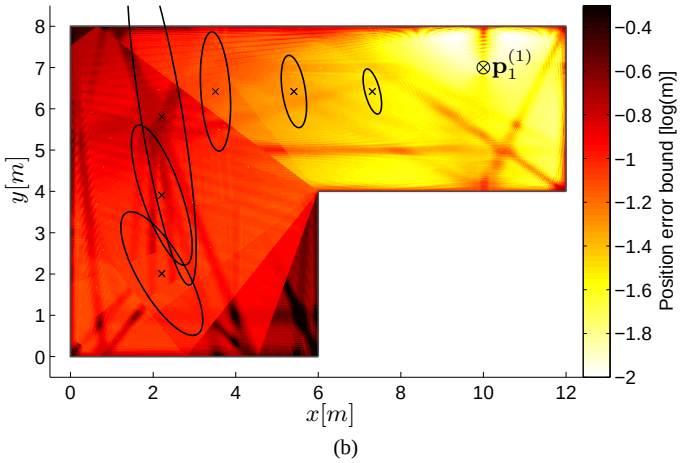

(b)

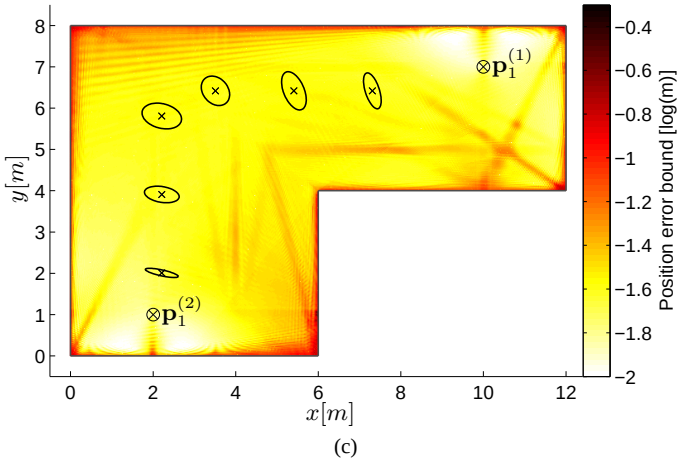

(c)

Fig. 2. Logarithmic PEB (10) for Multipath-ToA with $T_p = 1\,\text{ns}$ over the example room for VAs up to order two. (a) One anchor at $\mathbf{p}_1^{(1)}$; path overlap neglected. (b) same as (a) but considering the influence of path overlap. (c) a second anchor has been introduced at $\mathbf{p}_1^{(2)}$; path overlap included. At some sample points, 20-fold standard deviation ellipses are shown.

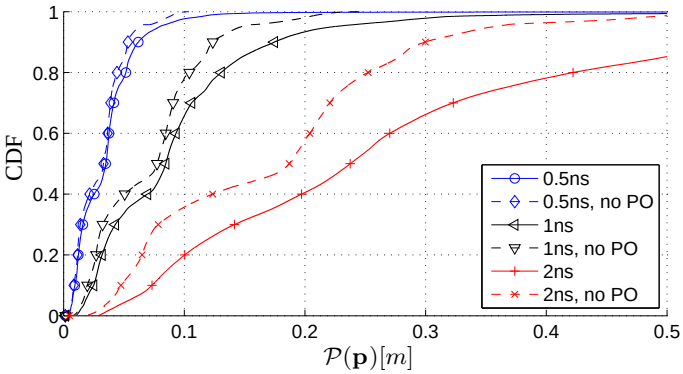

Fig. 3. CDFs of the PEB (10) for ToA, pulse durations $T_\text{p} = 0.5\,\text{ns}$, $T_\text{p} = 1\,\text{ns}$ and $T_\text{p} = 2\,\text{ns}$, and one anchor at $\mathbf{p}_1^{(1)}$. Path overlap is neglected in results marked by dashed lines.

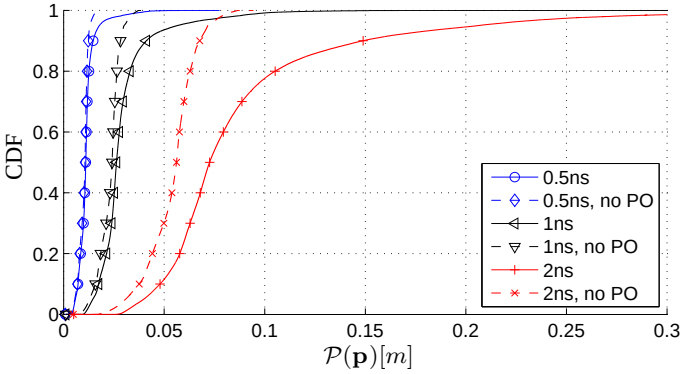

Fig. 4. CDFs of the PEB (10) for ToA, pulse durations $T_\text{p} = 0.5\,\text{ns}$, $T_\text{p} = 1\,\text{ns}$ and $T_\text{p} = 2\,\text{ns}$, and two anchors at $\mathbf{p}_1^{(1)}$ and $\mathbf{p}_1^{(2)}$. Path overlap is neglected in results marked by dashed lines.

B. *Multipath-TDoA*

Fig. 5 shows the CDFs of PEB (10) for Multipath-TDoA and different synchronization states, obtained from (30). The CDFs are shown for either two anchors at $\mathbf{p}_1^{(1)}$ and $\mathbf{p}_1^{(2)}$ which can be synchronized or not, or just the first anchor. A pulse duration of $T_\text{p} = 1\,\text{ns}$ is used and VAs up to order two are considered. The performance deteriorates w.r.t. the ToA case in Figs. 3 and 4, which can be explained by the fact that some of the delay information is used for clock-offset estimation, resulting in a loss of position-related information. A second anchor helps to counteract this effect. Here, one can recognize an additional gain of information if the two anchors are synchronized. The impact of path overlap is smaller if two anchors are used and even less pronounced if the anchors are synchronized.

A qualitative representation of the PEB over the example room is shown in Fig. 6, with two anchors at $\mathbf{p}_1^{(1)}$ and $\mathbf{p}_1^{(2)}$, $T_\text{p} = 1\,\text{ns}$, and VAs up to order two. By comparing this result with the ToA-PEB shown in Fig. 2(c), one can observe that the bound for TDoA is in general larger than for ToA. Also, the impact of path overlap is increased.

Fig. 7 compares ToA and TDoA for the two-anchors case and $T_\text{p} = 1\,\text{ns}$, considering VAs of order one or two, and also an NLOS scenario where the LOS component has been set to zero across the entire room. One can observe the importance of the LOS component which usually has a significantly larger SINR and provides thus more position-related information than MPCs arriving later. Increasing the VA order also leads to an information gain, except for very few positions, where it has a detrimental effect. The latter is explained by the fact that

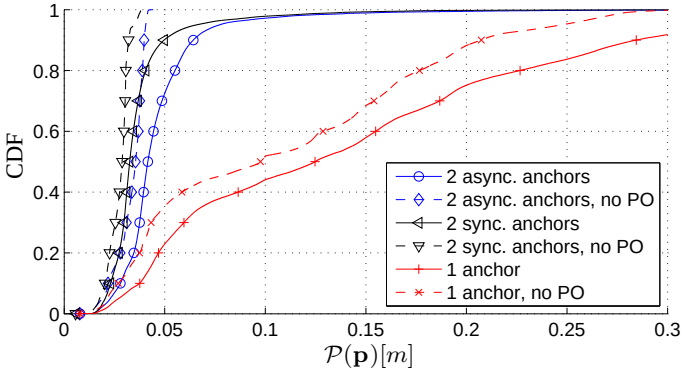

Fig. 5. CDFs of the PEB (10) for Multipath-TDoA and different synchronization settings at pulse duration $T_\mathrm{p} = 1\,\mathrm{ns}$, for VAs up to order two. Either two anchors are used at $\mathbf{p}_1^{(1)}$ and $\mathbf{p}_1^{(2)}$, which can be synchronized or not, or just the first anchor.

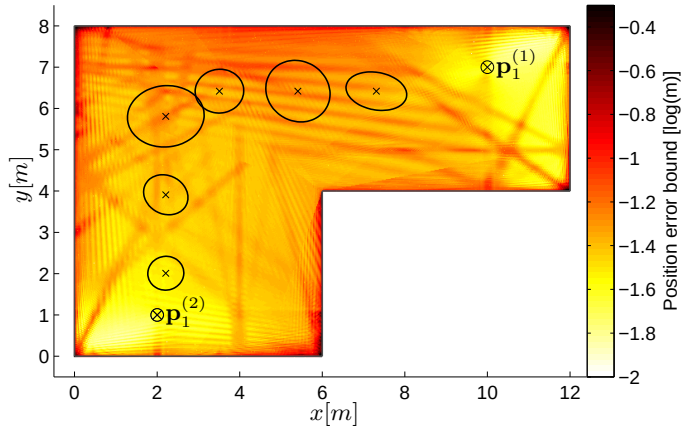

Fig. 6. Logarithmic PEB (10) for Multipath-TDoA over the example room with $T_\mathrm{p} = 1\,\mathrm{ns}$, using two asynchronous anchors at $\mathbf{p}_1^{(1)}$ and $\mathbf{p}_1^{(2)}$ and VAs up to order two. 20-fold standard deviation ellipses are shown at some sample points.

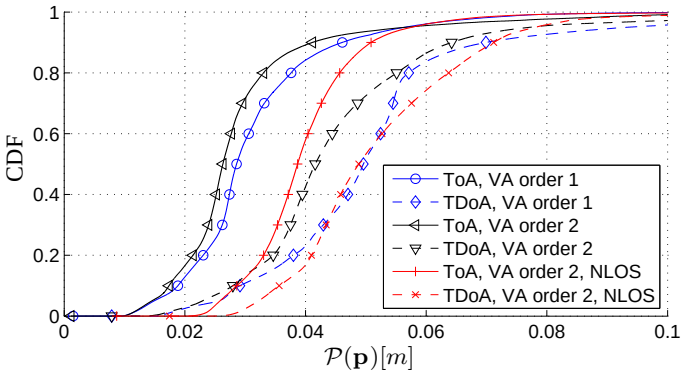

Fig. 7. CDFs of the PEB in (10) for ToA and TDoA and $T_\mathrm{p} = 1\,\mathrm{ns}$ with two anchors at $\mathbf{p}_1^{(1)}$ and $\mathbf{p}_1^{(2)}$. VAs of order one or two are considered; for the latter case also for an artificial NLOS situation over the whole room.

a larger VA order leads to more positions with unresolvable path overlap. This corresponds in Figs. 2(c) and 6 especially to locations close to walls and in corners.

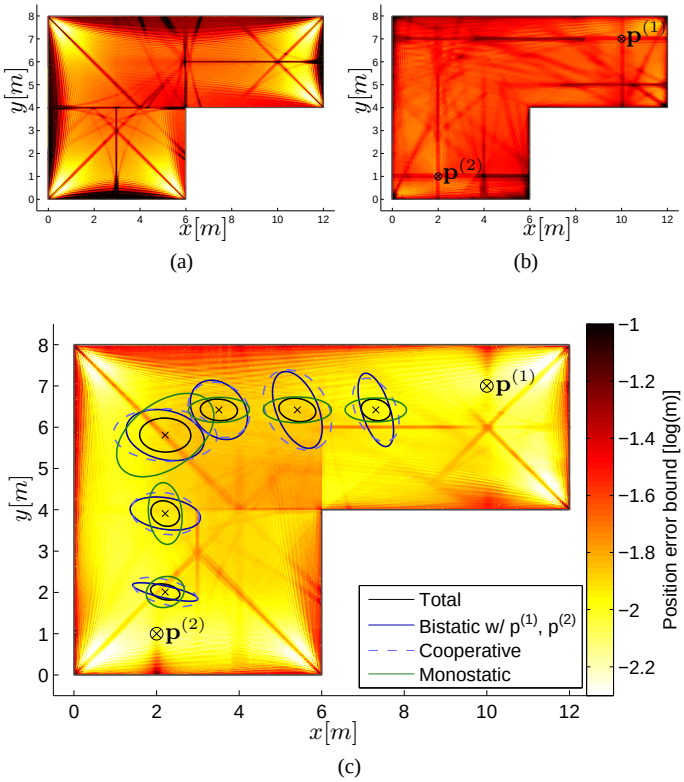

Fig. 8. Logarithmic PEB (41) with $T_\mathrm{p} = 1\,\mathrm{ns}$ over the example room for three cooperating agents, two of which are resting at positions $\mathbf{p}^{(1)}$ and $\mathbf{p}^{(2)}$. The PEB is decomposed into its (a) monostatic and (b) cooperative components. Plot (c) shows the total PEB for Multipath-Coop. In (c), also the 40-fold standard deviation ellipses are shown at some sample points for these three cases and—in addition—for the (bistatic) case with fixed anchors.

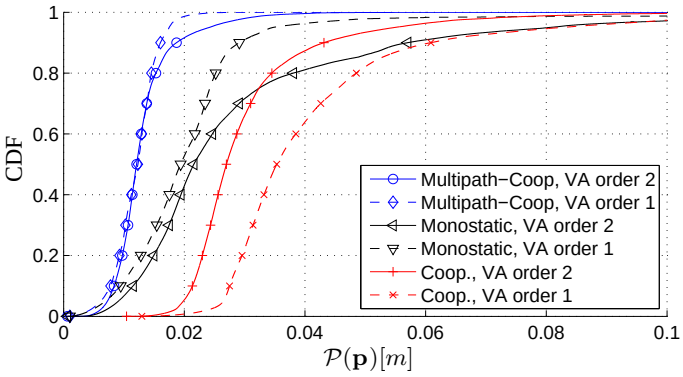

Fig. 9. CDFs of the PEB (41) for Multipath-Coop with $T_\mathrm{p} = 1\,\mathrm{ns}$, for VAs of order one and two, analyzing contributions of different measurements.

C. Multipath-Coop

Fig. 8 contains 2D-plots of the different contributions to the PEB in (41) for the cooperative case. The PEB has been evaluated for Agent 3 across the entire room with two resting, cooperating agents at $\mathbf{p}^{(1)}$ and $\mathbf{p}^{(2)}$, considering VAs up to order two. In Fig. 8(a), only the monostatic measurements of Agent 3 are considered, illustrating the adverse effect of room symmetries and resulting unresolvable path overlap. In particular, areas close to the walls are affected as well as the diagonals of the room. Fig. 8(b) shows the information

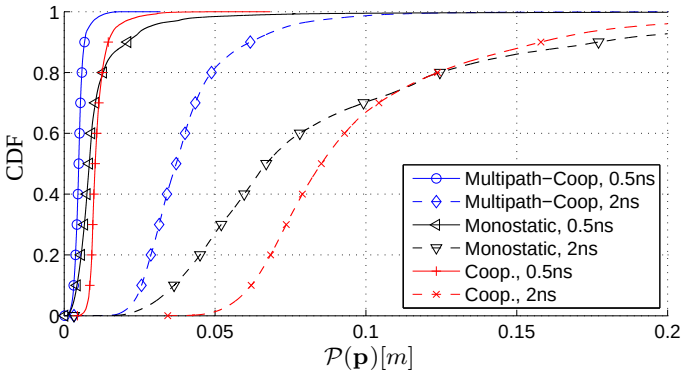

Fig. 10. CDFs of the PEB in (41) for Multipath-Coop with $T_\mathrm{p} = 0.5\,\mathrm{ns}$ and $T_\mathrm{p} = 2\,\mathrm{ns}$ for VAs of order two, showing contributions of different measurements types.

provided by the agents at $\mathbf{p}^{(1)}$ and $\mathbf{p}^{(2)}$ in their role as anchors. Their contribution is similar to the fixed-anchor case analyzed in Fig. 2(c), but due to uncertainties in their own positions, this information is not fully accessible. A robust, infrastructure-free positioning system is obtained if these two components can complement one another. Indeed Fig. 8(c) indicates excellent performance across the entire area. The distinction between the parts of the position-related information is further highlighted by the CRLB ellipses in Fig. 8(c), which also include the fixed-anchor (bistatic) case of Fig. 2(c). It shows the decreased information of the cooperative part in comparison to the bistatic case with fixed anchors. The monostatic ellipses are mostly oriented towards the nearest wall, where the most significant information comes from. In many cases, this seems to be nicely complemented by the cooperative contribution.

Fig. 9 shows the CDFs of the PEB in (41) for $T_\mathrm{p} = 1\,\mathrm{ns}$ and VAs of order one and two. It is interesting to note that Multipath-Coop does not benefit from taking into account second-order MPCs. This is explained by the large influence of the monostatic measurements, for which second-order reflections cause many regions with unresolvable path overlap (c.f. Fig. 8(a)). For cooperative measurements, increasing the VA order is still beneficial.

Fig. 10 illustrates the influence of bandwidth on Multipath-Coop, using $T_\mathrm{p} = 0.5\,\mathrm{ns}$ and $T_\mathrm{p} = 2\,\mathrm{ns}$ for VAs of order two. Especially for the monostatic measurements, the occurrence of unresolvable path overlap is significantly reduced, leading to a clear advantage of a larger bandwidth.

VII. Conclusions and Outlook

In this article, we have introduced a unified framework for evaluating the accuracy (and indirectly also the robustness) of radio-based indoor-localization methods that exploit geometric information contained in deterministic multipath components. The analysis shows and quantifies fundamental relationships between environment properties and the position-related information that can potentially be acquired. This is due to two mechanisms: (i) diffuse multipath, which is related to physical properties of the propagation environment, acts as interference to useful specular multipath components. (ii) path overlap, which relates to system design choices as the placement of agents but also to the given geometry of an environment, may render deterministic components useless. An increased signal bandwidth allows to counteract those effects since it improves the time-resolution of the measurements: The power of DM thus decreases and path overlap becomes less likely.

The framework allows for the analysis of different measurement setups: For instance, (i) in absence of synchronization, position information can be extracted from the time-difference between MPCs. The need for clock-offset estimation reduces thereby the positioning accuracy in comparison to a synchornized setup. (ii) Cooperation between agents increases the available position-related information, but the uncertainty of the unknown positions of agents *acting* as anchors partly levels this effect. (iii) With monostatic measurements, the VAs move synchronously with the agents, which leads to a scaling of the information provided by MPCs. These MPC-geometry-dependent scaling factors lie between zero and two w.r.t. a conventional bistatic measurement.

We have already shown that the quantification of position-related information, as provided by the presented framework, can be used efficiently for designing positioning and tracking algorithms (e.g. [22]–[24]). The proper parametrization of the underlying geometric-stochastic channel model optimizes such algorithms and provides valuable insight for system design choices such as antenna placements and signal parameters. Algorithms that can learn and extract these environmental parameters online from measurements may achieve such optimization without the need for manual system optimization and are thus an important topic for further research on robust indoor localization.

Appendix A
Likelihood Function for Orthogonal Pulses

For a sampled received signal, the covariance matrix of AWGN and the DM is written as

$$\mathbf{C}_\mathrm{n} = \sigma_\mathrm{n}^2 \mathbf{I}_N + \mathbf{C}_\mathrm{c} = \sigma_\mathrm{n}^2 \mathbf{I}_N + \bar{\mathbf{S}}^\mathrm{H} \mathbf{S}_\nu \bar{\mathbf{S}} \tag{A.1}$$

where the *full* signal matrix $\bar{\mathbf{S}} \in \mathbb{R}^{N\times N}$ is given by

$$\bar{\mathbf{S}} = \begin{bmatrix} \mathbf{s}_1^\mathrm{H} \\ \vdots \\ \mathbf{s}_N^\mathrm{H} \end{bmatrix} = \begin{bmatrix} s(T_\mathrm{s}-T_\mathrm{s}) & \dots & s(NT_\mathrm{s}-T_\mathrm{s}) \\ s(T_\mathrm{s}-2T_\mathrm{s}) & \dots & s(NT_\mathrm{s}-2T_\mathrm{s}) \\ \vdots & & \vdots \\ s(T_\mathrm{s}-NT_\mathrm{s}) & \dots & s(NT_\mathrm{s}-NT_\mathrm{s}) \end{bmatrix} \tag{A.2}$$

with $\mathbf{s}_i = \begin{bmatrix} s(T_\mathrm{s}-iT_\mathrm{s}) & \dots & s(NT_\mathrm{s}-iT_\mathrm{s}) \end{bmatrix}^\mathrm{H}$. So we can obtain for the covariance matrix of DM (c.f. Section III-A)

$$\begin{aligned} [\mathbf{C}_\mathrm{c}]_{n,m} &= [\bar{\mathbf{S}}^\mathrm{H} \mathbf{S}_\nu \bar{\mathbf{S}}]_{n,m} \\ &= \sum_{i=1}^{N} T_\mathrm{s} S_\nu(iT_\mathrm{s}) s(nT_\mathrm{s}-iT_\mathrm{s}) s(mT_\mathrm{s}-iT_\mathrm{s}). \end{aligned} \tag{A.3}$$

Using the Woodbury matrix identity, the inverse of the covariance matrix $\mathbf{C}_\mathrm{n}$ can be written as

$$\begin{aligned} \mathbf{Q}_\mathrm{n} &= \frac{1}{\sigma_\mathrm{n}^2}\mathbf{I}_N - \frac{1}{\sigma_\mathrm{n}^2}\bar{\mathbf{S}}^\mathrm{H}(\mathbf{S}_\nu^{-1} + \frac{1}{\sigma_\mathrm{n}^2}\bar{\mathbf{S}}\bar{\mathbf{S}}^\mathrm{H})^{-1}\bar{\mathbf{S}}\frac{1}{\sigma_\mathrm{n}^2} \\ &= \frac{1}{\sigma_\mathrm{n}^2}\mathbf{I}_N - \frac{1}{\sigma_\mathrm{n}^2}\bar{\mathbf{S}}^\mathrm{H}\mathbf{S}_\nu\left(\sigma_\mathrm{n}^2\mathbf{I}_N + \mathbf{S}_\nu\bar{\mathbf{S}}\bar{\mathbf{S}}^\mathrm{H}\right)^{-1}\bar{\mathbf{S}}. \end{aligned} \tag{A.4}$$

We now introduce the same assumptions as in [15], i.e. T_s is at Nyquist rate (denoted here as T_N), the transmit signal has a block spectrum, and the deterministic MPCs are orthogonal. This means that the full signal matrix $\bar{\mathbf{S}}$ is an orthogonal matrix with $\bar{\mathbf{S}}\bar{\mathbf{S}}^\mathrm{H} = \frac{1}{T_\mathrm{N}}\mathbf{I}_N$ and the signal matrix $\mathbf{S}$ is also orthogonal. So, (A.4) is given by

$$\mathbf{Q}_\mathrm{n} = \frac{1}{\sigma_\mathrm{n}^2}\mathbf{I}_N - \frac{1}{\sigma_\mathrm{n}^2}\bar{\mathbf{S}}^\mathrm{H}\mathbf{S}_\nu T_\mathrm{N}(N_0\mathbf{I}_N + \mathbf{S}_\nu)^{-1}\bar{\mathbf{S}} \tag{A.5}$$

which has a simple diagonal matrix to be inverted. We re-write the summands of likelihood function (7) using (A.5), yielding

$$\begin{aligned}\Re\left\{\mathbf{r}^\mathrm{H}\mathbf{Q}_\mathbf{n}\mathbf{S}\boldsymbol{\alpha}\right\} &= \Re\left\{\sum_{k=1}^{K}\alpha_k\mathbf{r}^\mathrm{H}\mathbf{Q}_\mathbf{n}\mathbf{s}_{\tau_k}\right\}\\ &= \Re\left\{\frac{1}{\sigma_\mathrm{n}^2}\sum_{k=1}^{K}\alpha_k\mathbf{r}^\mathrm{H}\Big(\mathbf{I}_N - \bar{\mathbf{S}}^\mathrm{H}\mathbf{S}_\nu T_\mathrm{N}\big(N_0\mathbf{I}_N + \mathbf{S}_\nu\big)^{-1}\bar{\mathbf{S}}\Big)\mathbf{s}_{\tau_k}\right\}\end{aligned} \tag{A.6}$$

and

$$\begin{aligned}\boldsymbol{\alpha}^\mathrm{H}\mathbf{S}^\mathrm{H}\mathbf{Q}_\mathbf{n}\mathbf{S}\boldsymbol{\alpha} &= \sum_{k=1}^{K}\sum_{k'=1}^{K}\alpha_k^*\alpha_{k'}\mathbf{s}_{\tau_k}^\mathrm{H}\mathbf{Q}_\mathbf{n}\mathbf{s}_{\tau_{k'}}\\ &= \frac{1}{\sigma_\mathrm{n}^2}\sum_{k=1}^{K}\sum_{k'=1}^{K}\alpha_k^*\alpha_{k'}\mathbf{s}_{\tau_k}^\mathrm{H}\Big(\mathbf{I}_N - \bar{\mathbf{S}}^\mathrm{H}\\ &\qquad\times\mathbf{S}_\nu T_\mathrm{N}\left(N_0\mathbf{I}_N + \mathbf{S}_\nu\right)^{-1}\bar{\mathbf{S}}\Big)\mathbf{s}_{\tau_{k'}}.\end{aligned} \tag{A.7}$$

The factor $\bar{\mathbf{S}}\mathbf{s}_{\tau_k}$ on the very right of these expressions is an autocorrelation vector of the transmitted signal shifted to delay time τ_k. The desired properties of $s(t)$—a large bandwidth and favorable autocorrelation properties—imply that this autocorrelation function has most of its energy concentrated at delay τ_k. It hence samples the nonstationary PDP at time τ_k and we can approximate for each summand

$$\bar{\mathbf{S}}^\mathrm{H}\mathbf{S}_\nu T_\mathrm{N}\big(N_0\mathbf{I}_N + T_\mathrm{N}\mathbf{S}_\nu\big)^{-1}\bar{\mathbf{S}} \approx \frac{T_\mathrm{N}S_\nu(\tau_k)}{N_0 + T_\mathrm{N}S_\nu(\tau_k)}\mathbf{I}_N.$$

With this approximation, (A.6) and (A.7) reduce to

$$\Re\left\{\mathbf{r}^\mathrm{H}\mathbf{Q}_\mathbf{n}\mathbf{S}\boldsymbol{\alpha}\right\} = \Re\left\{\frac{1}{\sigma_\mathrm{n}^2}\mathbf{r}^\mathrm{H}\sum_{k=1}^{K}w_k^2\alpha_k\mathbf{s}_{\tau_k}\right\}$$

and

$$\boldsymbol{\alpha}^\mathrm{H}\mathbf{S}^\mathrm{H}\mathbf{Q}_\mathbf{n}\mathbf{S}\boldsymbol{\alpha} = \frac{1}{\sigma_\mathrm{n}^2}\sum_{k=1}^{K}w_k^2|\alpha_k|^2\mathbf{s}_{\tau_k}^\mathrm{H}\mathbf{s}_{\tau_k}$$

respectively, where $w_k^2 = N_0/(N_0 + T_\mathrm{N}S_\nu(\tau_k))$. The double sum in (A.7) disappears due to the orthogonality of $\mathbf{S}$. So the likelihood function (7) can be re-written as (8), which is equivalent to (14) in [15].

Appendix B
Jacobian of VA Position w.r.t. Anchor Position

We want to find a simple expression for $\partial\mathbf{p}_k^{(\xi)}/\partial\mathbf{p}^{(\xi)}$. We restrict our derivation on a single VA of a specific node w.l.o.g., so we drop all ξ, k-indexing and use a simpler notation $\partial\mathbf{p}_\mathrm{VA}/\partial\mathbf{p}$. As explained in Section I, $\mathbf{p}_\mathrm{VA}$ is obtained by mirroring $\mathbf{p}$ on walls Q times where Q is the VA order. We use index q for this iteration and refer to the intermediate positions as $\tilde{\mathbf{p}}_q$ where $\tilde{\mathbf{p}}_0 = \mathbf{p}$ and $\tilde{\mathbf{p}}_Q = \mathbf{p}_\mathrm{VA}$. We need to express $\mathbf{p}_\mathrm{VA}$ as a function of $\mathbf{p}$ and room geometry. We account for the latter by considering walls with line equations

$$y - y_q = \tan(\gamma_q)\cdot(x - x_q) \tag{B.1}$$

where γ_q is the wall angle and $\mathbf{d}_q = (x_q, y_q)^\mathrm{T}$ is an offset vector. We obtain the q-th position by mirroring position $q-1$ on the q-th wall, or more formally

$$\tilde{\mathbf{p}}_q = \mathbf{Mir}(\tilde{\mathbf{p}}_{q-1}, \gamma_q, \mathbf{d}_q)\ . \tag{B.2}$$

where **Mir** is defined as the mirroring operator. Starting at $q = Q$ and by using recursive substitution down to $q = 0$, we get

$$\mathbf{p}_\mathrm{VA} = \mathbf{Mir}(\ldots\mathbf{Mir}(\mathbf{Mir}(\mathbf{p}, \gamma_1, \mathbf{d}_1), \gamma_2, \mathbf{d}_2)\ldots, \gamma_Q, \mathbf{d}_Q)\ . \tag{B.3}$$

The mirroring operation is given by

$$\begin{aligned}\mathbf{Mir}(\tilde{\mathbf{p}}_{q-1}, \gamma_q, \mathbf{d}_q) &= \mathbf{M}(\gamma_q)\cdot(\tilde{\mathbf{p}}_{q-1} - \mathbf{d}_q) + \mathbf{d}_q\\ &= \mathbf{M}(\gamma_q)\cdot\tilde{\mathbf{p}}_{q-1} + \big(\mathbf{I} - \mathbf{M}(\gamma_q)\big)\cdot\mathbf{d}_q\end{aligned} \tag{B.4}$$

where we use a mirror matrix that acts w.r.t. a line through the origin at angle γ_q,

$$\begin{aligned}\mathbf{M}(\gamma_q) &= \begin{bmatrix}\cos(2\gamma_q) & \sin(2\gamma_q)\\ \sin(2\gamma_q) & -\cos(2\gamma_q)\end{bmatrix}\\ &= \mathbf{Rot}(2\gamma_q)\begin{bmatrix}1 & 0\\ 0 & -1\end{bmatrix} = \mathbf{Rot}(2\gamma_q)\cdot\mathbf{F}\ .\end{aligned} \tag{B.5}$$

$\mathbf{M}(\gamma_q)$ has eigenvalues $\{-1, +1\}$ and bears analogies to rotation. $\mathbf{F}$ represents a sign-flip in the second dimension.

For breaking down (B.3), we prefer the latter form of (B.4) because of the separated $\tilde{\mathbf{p}}_{q-1}$-summand. By carefully repeated application, we obtain a formula

$$\begin{aligned}\mathbf{p}_\mathrm{VA} &= \mathbf{M}(\gamma_Q)\cdot\tilde{\mathbf{p}}_{Q-1} + \big(\mathbf{I} - \mathbf{M}(\gamma_Q)\big)\mathbf{d}_Q\\ &= \mathbf{M}(\gamma_Q)\mathbf{M}(\gamma_{Q-1})\cdot\tilde{\mathbf{p}}_{Q-2} +\\ &\quad\mathbf{M}(\gamma_Q)\big(\mathbf{I} - \mathbf{M}(\gamma_{Q-1})\big)\mathbf{d}_{Q-1} + \big(\mathbf{I} - \mathbf{M}(\gamma_Q)\big)\mathbf{d}_Q\\ &= \ \ldots\ = \Bigg(\prod_{q=0}^{Q-1}\mathbf{M}(\gamma_{Q-q})\Bigg)\mathbf{p} +\\ &\quad\sum_{q=1}^{Q}\Bigg(\prod_{\tilde{q}=1}^{Q-q}\mathbf{M}(\gamma_{Q+1-\tilde{q}})\Bigg)\left(\mathbf{I} - \mathbf{M}(\gamma_q)\right)\mathbf{d}_q\end{aligned} \tag{B.6}$$

where the derivative w.r.t. $\mathbf{p}$ is just the leading product of mirror matrices. Transposition reverses multiplication order

$$\left(\frac{\partial\mathbf{p}_\mathrm{VA}}{\partial\mathbf{p}}\right)^\mathrm{T} = \prod_{q=1}^{Q}\mathbf{M}(\gamma_q)\ . \tag{B.7}$$

To resolve this product, we derive a pseudo-homomorphism property of the mirror matrix. We note that both $\mathbf{F}$ and $\mathbf{M}(\gamma)$ are symmetric, orthogonal, and self-inverse. Thus, $\mathbf{M}(\gamma) = \mathbf{Rot}(2\gamma)\cdot\mathbf{F}$ implies $\mathbf{M}(\gamma)\cdot\mathbf{F} = \mathbf{Rot}(2\gamma)$. We rearrange the product of two mirror matrices

$$\begin{aligned}\mathbf{M}(\gamma)\mathbf{M}(\beta) &= \mathbf{M}(\gamma)\mathbf{M}(\beta)^\mathrm{T} = \mathbf{Rot}(2\gamma)\mathbf{F}\mathbf{F}^\mathrm{T}\mathbf{Rot}(2\beta)^\mathrm{T}\\ &= \mathbf{Rot}(2\gamma)\cdot\mathbf{I}\cdot\mathbf{Rot}(-2\beta) = \mathbf{Rot}(2(\gamma - \beta))\end{aligned}$$

and obtain the property

$$\mathbf{M}(\gamma)\mathbf{M}(\beta) = \mathbf{M}(\gamma-\beta)\cdot\mathbf{F}\ . \tag{B.8}$$

Applying (B.8) to (B.7) $(Q-1)$-times yields

$$\left(\frac{\partial \mathbf{p}_{\mathrm{VA}}}{\partial \mathbf{p}}\right)^{\mathrm{T}} = \mathbf{M}(\bar{\gamma})\cdot\mathbf{F}^{Q-1} = \mathbf{Rot}(2\bar{\gamma})\cdot\mathbf{F}^{Q} \tag{B.9}$$

where we refer to $\bar{\gamma} := \gamma_1 - \gamma_2 + \ldots + (-1)^{Q-1}\cdot\gamma_Q$ as the effective wall angle.

Appendix C
Delay Gradient for the Monostatic Setup

We transform the initial gradient from Appendix B into a magnitude-times-unit-vector form by component-wise application of basic trigonometric identities. This yields an insightful expression for the monostatic case, cf. (20). We consider

$$\mathbf{e}(\phi) - \mathbf{e}((-1)^Q\phi + 2\bar{\gamma}) = \begin{bmatrix}\cos(\phi) - \cos((-1)^Q\phi + 2\bar{\gamma})\\ \sin(\phi) - \sin((-1)^Q\phi + 2\bar{\gamma})\end{bmatrix}$$
$$= \begin{bmatrix} 2\sin\left(\frac{((-1)^Q+1)\phi+2\bar{\gamma}}{2}\right)\sin\left(\frac{((-1)^Q-1)\phi+2\bar{\gamma}}{2}\right)\\ 2\cos\left(\frac{((-1)^Q+1)\phi+2\bar{\gamma}}{2}\right)\sin\left(-\frac{((-1)^Q-1)\phi+2\bar{\gamma}}{2}\right)\end{bmatrix}.$$

By defining symbols for the arguments that contain ϕ depending on the even/odd parity of Q

$$O := \frac{(-1)^Q-1}{2}\phi + \bar{\gamma} = \begin{cases}\bar{\gamma} & \text{If } Q \text{ is even}\\ \bar{\gamma}-\phi & \text{If } Q \text{ is odd}\end{cases}$$
$$E := \frac{(-1)^Q+1}{2}\phi + \bar{\gamma} = \begin{cases}\bar{\gamma}+\phi & \text{If } Q \text{ is even}\\ \bar{\gamma} & \text{If } Q \text{ is odd}\end{cases}$$

we further get

$$\mathbf{e}(\phi) - \mathbf{e}((-1)^Q\phi + 2\bar{\gamma}) = 2\sin(O)\begin{bmatrix}\sin(E)\\ -\cos(E)\end{bmatrix}$$
$$= 2\sin(O)\ \mathbf{e}\Big(E - \frac{\pi}{2}\Big)$$
$$= \begin{cases} 2\sin(\bar{\gamma})\mathbf{e}(\phi+\bar{\gamma}-\frac{\pi}{2}) & \text{If } Q \text{ is even}\\ 2\sin(\bar{\gamma}-\phi)\mathbf{e}(\bar{\gamma}-\frac{\pi}{2}) & \text{If } Q \text{ is odd}\end{cases}. \tag{C.1}$$

Appendix D
FIM for Orthogonal Pulses

If we assume no path overlap (i.e. orthogonality) between signals from different VAs, $\mathbf{\Lambda}_{\mathrm{B}} = \mathbf{0}$ and $\mathbf{\Lambda}_{\mathrm{A}}$ is a diagonal matrix. Using the resulting likelihood function (8) derived in Appendix A, $\mathbf{\Lambda}_{\mathrm{A}}$ can be rewritten as

$$[\mathbf{\Lambda}_{\mathrm{A}}]_{k,k} = \mathbb{E}_{\mathbf{r}|\boldsymbol{\psi}}\left\{-\frac{\partial^2 \ln f(\mathbf{r}|\boldsymbol{\psi})}{\partial\tau_k\partial\tau_k}\right\} \tag{D.1}$$
$$= 2\Re\left\{\frac{|\alpha_k|^2 w_k^2}{\sigma_{\mathrm{n}}^2}\left(\frac{\partial \mathbf{s}_{\tau_k}}{\partial\tau_k}\right)^{\mathrm{H}}\frac{\partial \mathbf{s}_{\tau_k}}{\partial\tau_k}\right\}$$
$$= 2\Re\left\{\frac{|\alpha_k|^2 w_k^2}{\sigma_{\mathrm{n}}^2}\frac{\partial^2}{\partial\tau_k^2}\sum_{i=1}^{N} s(iT_{\mathrm{s}}-\tau_k)s(iT_{\mathrm{s}}-\tau_k)\right\}$$

Approximating the sum by an integral, we get

$$[\mathbf{\Lambda}_{\mathrm{A}}]_{k,k} \approx 2\Re\left\{\frac{|\alpha_k|^2 w_k^2}{\sigma_{\mathrm{n}}^2}\frac{\partial^2}{\partial\tau_k^2}\frac{1}{T_{\mathrm{s}}}\int_0^{NT_{\mathrm{s}}} s(t-\tau_k)s(t-\tau_k)\mathrm{d}t\right\}$$
$$= 2\Re\left\{\frac{|\alpha_k|^2 w_k^2}{\sigma_{\mathrm{n}}^2 T_{\mathrm{s}}}\int_f |2\pi f|^2|S(f)|^2\mathrm{d}f\right\}$$
$$= 8\pi^2\beta^2|\alpha_k|^2 w_k^2/N_0$$

where $\beta = \int_f f^2|S(f)|^2\mathrm{d}f$ is the effective (mean square) bandwidth for $s(t)$ normalized to unit energy.

Appendix E
Derivation of the TDoA CRLB

Synchronized anchors: In order to derive the 3×3 EFIM $\boldsymbol{\mathcal{I}}_{\mathbf{p},\epsilon}$ we need to repartition the transformation matrix $\mathbf{J}$ by combining the submatrices $\mathbf{H}^{(j)}$ and $\mathbf{L}^{(j)} = \mathbf{l}_{\text{syn}}^{(j)}$ to $\mathbf{G}^{(j)} = [\mathbf{H}^{(j)}, \mathbf{l}_{\text{syn}}^{(j)}]$. Applying the transformation leads to

$$\boldsymbol{\mathcal{I}}_{\boldsymbol{\theta}} = \mathbf{J}^{\mathrm{T}}\boldsymbol{\mathcal{I}}_{\boldsymbol{\psi}}\mathbf{J} = \tag{E.1}$$
$$\begin{bmatrix}\sum\limits_{j\in\mathcal{N}_j}\left(\mathbf{G}^{(j)}\right)^{\mathrm{T}}\mathbf{\Lambda}_{\mathrm{A}}^{(j)}\mathbf{G}^{(j)} & \left(\mathbf{G}^{(1)}\right)^{\mathrm{T}}\mathbf{\Lambda}_{\mathrm{B}}^{(1)} & \cdots & \left(\mathbf{G}^{(J)}\right)^{\mathrm{T}}\mathbf{\Lambda}_{\mathrm{B}}^{(J)}\\ \left(\mathbf{\Lambda}_{\mathrm{B}}^{(1)}\right)^{\mathrm{T}}\mathbf{G}^{(1)} & \mathbf{\Lambda}_{\mathrm{C}}^{(1)} & & \\ \vdots & & \ddots & \\ \left(\mathbf{\Lambda}_{\mathrm{B}}^{(J)}\right)^{\mathrm{T}}\mathbf{G}^{(J)} & & & \mathbf{\Lambda}_{\mathrm{C}}^{(J)}\end{bmatrix}.$$

The 3×3 EFIM is then given as the sum over the EFIMs of the corresponding anchors

$$\boldsymbol{\mathcal{I}}_{\mathbf{p},\epsilon} = \sum_{j\in\mathcal{N}_j}\left(\mathbf{G}^{(j)}\right)^{\mathrm{T}}\Big[\mathbf{\Lambda}_{\mathrm{A}}^{(j)} - \mathbf{\Lambda}_{\mathrm{B}}^{(j)}\left(\mathbf{\Lambda}_{\mathrm{C}}^{(j)}\right)^{-1}\left(\mathbf{\Lambda}_{\mathrm{B}}^{(j)}\right)^{\mathrm{T}}\Big]\mathbf{G}^{(j)}. \tag{E.2}$$

When neglecting path overlap, this reduces to

$$\boldsymbol{\mathcal{I}}_{\mathbf{p},\epsilon} = \sum_{j\in\mathcal{N}_j}\left(\mathbf{G}^{(j)}\right)^{\mathrm{T}}\mathbf{\Lambda}_{\mathrm{A}}^{(j)}\mathbf{G}^{(j)}, \tag{E.3}$$

which leads finally to (29).

Asynchronous anchors: The result for $\boldsymbol{\mathcal{I}}_{\boldsymbol{\theta}}$ (E.1) is also valid when considering asynchronous anchors, provided that we respect $\mathbf{L}^{(j)} = \mathbf{L}_{\text{asyn}}^{(j)}$ and $\mathbf{G}^{(j)} = [\mathbf{H}^{(j)}, \mathbf{L}_{\text{asyn}}^{(j)}]$. We apply the blockwise inversion lemma twice, first to derive the EFIM $\boldsymbol{\mathcal{I}}_{\mathbf{p},\boldsymbol{\epsilon}}$ (note that now $\boldsymbol{\epsilon}$ is a vector), and then again to proof the additivity of the EFIMs $\boldsymbol{\mathcal{I}}_{\mathbf{p}}^{(j)}$.

The EFIM $\boldsymbol{\mathcal{I}}_{\mathbf{p},\boldsymbol{\epsilon}}$ is now a square matrix of order $2+J$. It can be expressed as in (E.2), but taking account of the changed definition of $\mathbf{G}^{(j)}$. We can write its structure as

$$\boldsymbol{\mathcal{I}}_{\mathbf{p},\boldsymbol{\epsilon}} = \sum_{j\in\mathcal{N}_j}\begin{bmatrix}\boldsymbol{\mathcal{I}}_A^{(j)} & \boldsymbol{\mathcal{I}}_B^{(j)}\\ \left(\boldsymbol{\mathcal{I}}_B^{(j)}\right)^{\mathrm{T}} & \boldsymbol{\mathcal{I}}_D^{(j)}\end{bmatrix}, \tag{E.4}$$

with $\boldsymbol{\mathcal{I}}_A^{(j)} \in \mathbb{R}^{2\times 2}$, $\boldsymbol{\mathcal{I}}_B^{(j)} \in \mathbb{R}^{2\times J}$ and $\boldsymbol{\mathcal{I}}_D^{(j)} \in \mathbb{R}^{J\times J}$. Further evaluation yields, that only the j-th column of $\boldsymbol{\mathcal{I}}_B^{(j)}$ is nonzero, and the sum over $\boldsymbol{\mathcal{I}}_B^{(j)}$ can be written as

$$\sum_{j\in\mathcal{N}_j}\boldsymbol{\mathcal{I}}_B^{(j)} = \left[\mathbf{b}^{(1)},\ldots,\mathbf{b}^{(J)}\right],\ \mathbf{b}^{(j)}\in\mathbb{R}^2, \tag{E.5}$$

meaning that each column is determined by the contribution of a different anchors. Similarly, $\boldsymbol{\mathcal{I}}_D^{(j)}$ has only one nonzero entry $\left[\boldsymbol{\mathcal{I}}_D^{(j)}\right]_{j,j}$, leading to

$$\sum_{j\in\mathcal{N}_j}\boldsymbol{\mathcal{I}}_D^{(j)} = \operatorname{diag}\left(\left[\boldsymbol{\mathcal{I}}_D^{(1)}\right]_{1,1},\dots,\left[\boldsymbol{\mathcal{I}}_D^{(J)}\right]_{J,J}\right). \tag{E.6}$$

Rewriting $\boldsymbol{\mathcal{I}}_{\mathbf{p},\boldsymbol{\epsilon}}$ (E.4) and again applying the blockwise inversion lemma yields the additivity of the EFIMs $\boldsymbol{\mathcal{I}}_{\mathbf{p}}^{(j)}$:

$$\boldsymbol{\mathcal{I}}_{\mathbf{p}} = \sum_{j\in\mathcal{N}_j}\boldsymbol{\mathcal{I}}_A^{(j)} - \frac{1}{\left[\boldsymbol{\mathcal{I}}_D^{(j)}\right]_{j,j}}\mathbf{b}^{(j)}\left(\mathbf{b}^{(j)}\right)^{\mathrm{T}} = \sum_{j\in\mathcal{N}_j}\boldsymbol{\mathcal{I}}_{\mathbf{p}}^{(j)}. \tag{E.7}$$

The involved terms are defined by

$$\boldsymbol{\mathcal{I}}_A^{(j)} = \left(\mathbf{H}^{(j)}\right)^{\mathrm{T}}\left(\boldsymbol{\Lambda}_{\mathrm{A}}^{(j)} - \boldsymbol{\Lambda}_{\mathrm{B}}^{(j)}\left(\boldsymbol{\Lambda}_{\mathrm{C}}^{(j)}\right)^{-1}\left(\boldsymbol{\Lambda}_{\mathrm{B}}^{(j)}\right)^{\mathrm{T}}\right)\mathbf{H}^{(j)},$$

$$\left[\boldsymbol{\mathcal{I}}_D^{(j)}\right]_{j,j} = \sum_{u=1}^{K^{(j)}}\sum_{v=1}^{K^{(j)}}\left[\boldsymbol{\Lambda}_{\mathrm{A}}^{(j)} - \boldsymbol{\Lambda}_{\mathrm{B}}^{(j)}\left(\boldsymbol{\Lambda}_{\mathrm{C}}^{(j)}\right)^{-1}\left(\boldsymbol{\Lambda}_{\mathrm{B}}^{(j)}\right)^{\mathrm{T}}\right]_{u,v},$$

and

$$\mathbf{b}^{(j)} = \left(\mathbf{H}^{(j)}\right)^{\mathrm{T}}\left(\boldsymbol{\Lambda}_{\mathrm{A}}^{(j)} - \boldsymbol{\Lambda}_{\mathrm{B}}^{(j)}\left(\boldsymbol{\Lambda}_{\mathrm{C}}^{(j)}\right)^{-1}\left(\boldsymbol{\Lambda}_{\mathrm{B}}^{(j)}\right)^{\mathrm{T}}\right)[1\dots1]^{\mathrm{T}}_{1\times K^{(J)}}.$$

Appendix F
Derivation of the Multipath-Coop CRLB

The EFIM for the cooperative setup is defined as

$$\boldsymbol{\mathcal{I}}_{\mathbf{P}} = \mathbf{H}^{\mathrm{T}}\operatorname{diag}\left(\boldsymbol{\Lambda}^{(1,1)},\dots,\boldsymbol{\Lambda}^{(1,M)},\dots,\boldsymbol{\Lambda}^{(M+J,M)}\right)\mathbf{H}, \tag{F.1}$$

being of size $2M\times 2M$. It can be written with subblock $\mathbf{H}$ from (39) in the canonical form (37). Matrix $\boldsymbol{\Lambda}^{(j,m)}$ is defined in (38). The canonical form decomposes the EFIM $\boldsymbol{\mathcal{I}}_{\mathbf{P}}$ into contributions from independent transmissions inbetween the agents or between agents and fixed anchors. Matrix $\boldsymbol{\mathcal{I}}_{\mathbf{P}}$ consists of the following subblocks for $\eta,\eta'\in\mathcal{N}_m=\{1,\dots,M\}$,

$$[\boldsymbol{\mathcal{I}}_{\mathbf{P}}]_{2\times2}^{\eta,\eta'} = \sum_{j\in(\mathcal{N}_m\cup\mathcal{N}_j)}\sum_{m\in\mathcal{N}_m}\left(\mathbf{H}^{(j,\eta,m)}\right)^{\mathrm{T}}\boldsymbol{\Lambda}^{(j,m)}\mathbf{H}^{(j,\eta',m)} \tag{F.2}$$

where $\mathbf{H}^{(j,\eta,m)}$ stacks the spatial delay gradients (17) as defined in Section IV. Considering that only summand (j,m) of (F.2) contributes to a block, for which either index j or index m equals η or η', we get the following subblocks:

1) Off-diagonal blocks $\eta\neq\eta'$:

$$\begin{aligned}[\boldsymbol{\mathcal{I}}_{\mathbf{P}}]_{2\times2}^{(\eta,\eta')} &= \left(\mathbf{H}^{(j,\eta,m)}\right)^{\mathrm{T}}\boldsymbol{\Lambda}^{(j,m)}\mathbf{H}^{(j,\eta',m)}\Big|_{j=\eta,m=\eta'}\\ &\quad+\left(\mathbf{H}^{(j,\eta,m)}\right)^{\mathrm{T}}\boldsymbol{\Lambda}^{(j,m)}\mathbf{H}^{(j,\eta',m)}\Big|_{j=\eta',m=\eta}\\ &= \left(\mathbf{H}_{\mathrm{An}}^{(\eta,\eta')}\right)^{\mathrm{T}}\boldsymbol{\Lambda}^{(\eta,\eta')}\mathbf{H}_{\mathrm{Ag}}^{(\eta',\eta)}\\ &\quad+\left(\mathbf{H}_{\mathrm{Ag}}^{(\eta',\eta)}\right)^{\mathrm{T}}\boldsymbol{\Lambda}^{(\eta',\eta)}\mathbf{H}_{\mathrm{An}}^{(\eta',\eta)},\end{aligned}$$

using the definitions for $\mathbf{H}_{\mathrm{An}}^{(\eta,\eta')}$ and $\mathbf{H}_{\mathrm{Ag}}^{(\eta,\eta')}$ from Section IV-1. With $\mathbf{H}_{\mathrm{An}}^{(\eta,\eta')}=\mathbf{H}_{\mathrm{Ag}}^{(\eta',\eta)}$ (Section IV-1) and $\boldsymbol{\Lambda}^{(\eta,\eta')}=\boldsymbol{\Lambda}^{(\eta',\eta)}$ we get

$$[\boldsymbol{\mathcal{I}}_{\mathbf{P}}]_{2\times2}^{(\eta,\eta')} = 2\boldsymbol{\mathcal{I}}_{\mathrm{C}}^{(\eta,\eta')} = 2\left(\mathbf{H}_{\mathrm{Ag}}^{(\eta',\eta)}\right)^{\mathrm{T}}\boldsymbol{\Lambda}^{(\eta',\eta)}\mathbf{H}_{\mathrm{Ag}}^{(\eta,\eta')}. \tag{F.3}$$

2) Diagonal blocks $\eta=\eta'$:

$$\begin{aligned}[\boldsymbol{\mathcal{I}}_{\mathbf{P}}]_{2\times2}^{\eta,\eta} &= \left(\mathbf{H}^{(\eta,\eta,\eta)}\right)^{\mathrm{T}}\boldsymbol{\Lambda}^{(\eta,\eta)}\mathbf{H}^{(\eta,\eta,\eta)}\\ &\quad+\sum_{\substack{j\in\mathcal{N}_m\setminus\{\eta\}\\ m=\eta}}\left(\mathbf{H}^{(j,\eta,m)}\right)^{\mathrm{T}}\boldsymbol{\Lambda}^{(j,m)}\mathbf{H}^{(j,\eta,m)}\\ &\quad+\sum_{\substack{m\in\mathcal{N}_m\setminus\{\eta\}\\ j=\eta}}\left(\mathbf{H}^{(j,\eta,m)}\right)^{\mathrm{T}}\boldsymbol{\Lambda}^{(j,m)}\mathbf{H}^{(j,\eta,m)}\\ &\quad+\sum_{j\in\mathcal{N}_j}\left(\mathbf{H}^{(j,\eta,\eta)}\right)^{\mathrm{T}}\boldsymbol{\Lambda}^{(j,\eta)}\mathbf{H}^{(j,\eta,\eta)}\\ &= \left(\mathbf{H}_{\mathrm{Mo}}^{(\eta)}\right)^{\mathrm{T}}\boldsymbol{\Lambda}^{(\eta,\eta)}\mathbf{H}_{\mathrm{Mo}}^{(\eta)}\\ &\quad+\sum_{j\in\mathcal{N}_m\setminus\{\eta\}}\left(\mathbf{H}_{\mathrm{Ag}}^{(j,\eta)}\right)^{\mathrm{T}}\boldsymbol{\Lambda}^{(j,\eta)}\mathbf{H}_{\mathrm{Ag}}^{(j,\eta)}\\ &\quad+\sum_{m\in\mathcal{N}_m\setminus\{\eta\}}\left(\mathbf{H}_{\mathrm{An}}^{(\eta,m)}\right)^{\mathrm{T}}\boldsymbol{\Lambda}^{(\eta,m)}\mathbf{H}_{\mathrm{An}}^{(\eta,m)}\\ &\quad+\sum_{j\in\mathcal{N}_j}\left(\mathbf{H}_{\mathrm{Ag}}^{(j,\eta)}\right)^{\mathrm{T}}\boldsymbol{\Lambda}^{(j,\eta)}\mathbf{H}_{\mathrm{Ag}}^{(j,\eta)}\end{aligned}$$

using again $\mathbf{H}_{\mathrm{An}}^{(\eta,\eta')}$ and $\mathbf{H}_{\mathrm{Ag}}^{(\eta,\eta')}$ from Section IV-1 and $\mathbf{H}_{\mathrm{Mo}}^{(\eta)}$ from Section IV-2. With $\mathbf{H}_{\mathrm{An}}^{(\eta,m)}=\mathbf{H}_{\mathrm{Ag}}^{(m,\eta)}$ and $\boldsymbol{\Lambda}^{(j,m)}=\boldsymbol{\Lambda}^{(m,j)}$ due to reciprocity, we get

$$\begin{aligned}[\boldsymbol{\mathcal{I}}_{\mathbf{P}}]_{2\times2}^{(\eta,\eta)} &= \boldsymbol{\mathcal{I}}_{\mathrm{Mo}}^{(\eta)} + 2\sum_{m\in\mathcal{N}_m\setminus\{\eta\}}\boldsymbol{\mathcal{I}}_{\mathrm{Ag}}^{(m,\eta)} + \sum_{j\in\mathcal{N}_j}\boldsymbol{\mathcal{I}}_{\mathrm{An}}^{(j,\eta)}\\ &= \boldsymbol{\mathcal{I}}_{\mathrm{Mo}}^{(\eta)} + 2\boldsymbol{\mathcal{I}}_{\mathrm{Ag}}^{(\eta)} + \boldsymbol{\mathcal{I}}_{\mathrm{An}}^{(\eta)}\end{aligned} \tag{F.4}$$

which implicitly defines the contributions from monostatic measurements, bistatic measurements in between agents, and bistatic measurements between agents and fixed anchors.

References

[1] Y. Shen, S. Mazuelas, and M. Win, "Network Navigation: Theory and Interpretation," *IEEE Journal on Selected Areas in Communications*, 2012.

[2] A. Conti, D. Dardari, M. Guerra, L. Mucchi, and M. Win, "Experimental Characterization of Diversity Navigation," *IEEE Systems Journal*, 2014.

[3] S. Marano and, W. Gifford, H. Wymeersch, and M. Win, "NLOS identification and mitigation for localization based on UWB experimental data," *IEEE Journal on Selected Areas in Communications*, 2010.

[4] H. Wymeersch, S. Marano, W. Gifford, and M. Win, "A Machine Learning Approach to Ranging Error Mitigation for UWB Localization," *IEEE Transactions on Communications*, 2012.

[5] H. Lu, S. Mazuelas, and M. Win, "Ranging likelihood for wideband wireless localization," in *IEEE International Conference on Communications (ICC)*, 2013.

[6] H. Wymeersch, J. Lien, and M. Z. Win, "Cooperative Localization in Wireless Networks," *Proceedings of the IEEE*, 2009.

[7] Y. Shen and M. Win, "On the Use of Multipath Geometry for Wideband Cooperative Localization," in *IEEE Global Telecommunications Conference (GLOBECOM)*, 2009.

[8] R. Parhizkar, I. Dokmanic, and M. Vetterli, "Single-Channel Indoor Microphone Localization," in *39th International Conference on Acoustics, Speech, and Signal Processing*, 2014.

[9] M. Leigsnering, M. Amin, F. Ahmad, and A. Zoubir, "Multipath Exploitation and Suppression for SAR Imaging of Building Interiors: An overview of recent advances," *IEEE Signal Processing Magazine*, 2014.

[10] I. Dokmanic, R. Parhizkar, A. Walther, Y. M. Lu, and M. Vetterli, "Acoustic Echoes Reveal Room Shape," *Proceedings of the National Academy of Sciences*, 2013.

[11] P. Meissner and K. Witrisal, "Analysis of Position-Related Information in Measured UWB Indoor Channels," in *6th European Conference on Antennas and Propagation (EuCAP)*, 2012.

[12] Y. Shen and M. Win, "Fundamental Limits of Wideband Localization; Part I: A General Framework," *IEEE Transactions on Information Theory*, 2010.

[13] Y. Shen, H. Wymeersch, and M. Win, "Fundamental Limits of Wideband Localization - Part II: Cooperative Networks," *IEEE Transactions on Information Theory*, 2010.

[14] H. Godrich, A. Haimovich, and R. Blum, "Target Localization Accuracy Gain in MIMO Radar-Based Systems," *IEEE Transactions on Information Theory*, vol. 56, no. 6, pp. 2783 –2803, June 2010.

[15] K. Witrisal and P. Meissner, "Performance bounds for multipath-assisted indoor navigation and tracking (MINT)," in *IEEE International Conference on Communications (ICC)*, 2012.

[16] H. L. Van Trees, *Detection, Estimation and Modulation, Part I*. Wiley Press, 1968.

[17] A. Richter and R. Thoma, "Joint maximum likelihood estimation of specular paths and distributed diffuse scattering," in *IEEE Vehicular Technology Conference, VTC 2005-Spring*, 2005.

[18] N. Michelusi, U. Mitra, A. Molisch, and M. Zorzi, "UWB Sparse/Diffuse Channels, Part I: Channel Models and Bayesian Estimators," *IEEE Transactions on Signal Processing*, 2012.

[19] N. Decarli, F. Guidi, and D. Dardari, "A Novel Joint RFID and Radar Sensor Network for Passive Localization: Design and Performance Bounds," *IEEE Journal of Selected Topics in Signal Processing*, 2014.

[20] T. Santos, F. Tufvesson, and A. Molisch, "Modeling the Ultra-Wideband Outdoor Channel: Model Specification and Validation," *IEEE Transactions on Wireless Communications*, 2010.

[21] J. Karedal, S. Wyne, P. Almers, F. Tufvesson, and A. Molisch, "A Measurement-Based Statistical Model for Industrial Ultra-Wideband Channels," *IEEE Transactions on Wireless Communications*, 2007.

[22] P. Meissner, E. Leitinger, and K. Witrisal, "UWB for robust indoor tracking: Weighting of multipath components for efficient estimation," *IEEE Wireless Communications Letters*, 2014, in press.

[23] P. Meissner, E. Leitinger, M. Lafer, and K. Witrisal, "Real-Time Demonstration System for Multipath-Assisted Indoor Navigation and Tracking (MINT)," in *IEEE ICC 2014 Workshop on Advances in Network Localization and Navigation (ANLN)*, 2014.

[24] E. Leitinger, M. Froehle, P. Meissner, and K. Witrisal, "Multipath-Assisted Maximum-Likelihood Indoor Positioning using UWB Signals," in *IEEE ICC 2014 Workshop on Advances in Network Localization and Navigation (ANLN)*, 2014.

[25] J. Borish, "Extension of the image model to arbitrary polyhedra," *The Journal of the Acoustical Society of America*, 1984.

[26] J. Kunisch and J. Pamp, "An ultra-wideband space-variant multipath indoor radio channel model," in *IEEE Conference on Ultra Wideband Systems and Technologies*, 2003.

[27] M. Froehle, E. Leitinger, P. Meissner, and K. Witrisal, "Cooperative Multipath-Assisted Indoor Navigation and Tracking (Co-MINT) Using UWB Signals," in *IEEE ICC 2013 Workshop on Advances in Network Localization and Navigation (ANLN)*, 2013.

[28] A. Molisch, "Ultra-wide-band propagation channels," *Proceedings of the IEEE*, 2009.

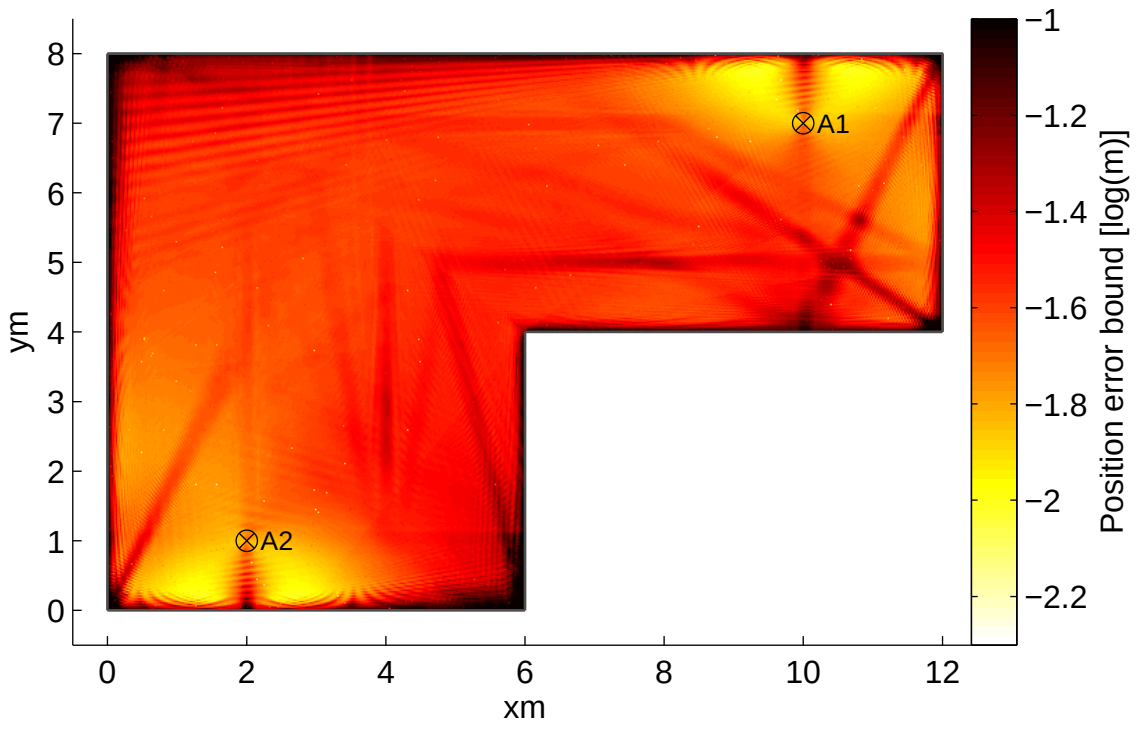
A1
A2
ym
xm
0
2
4
6
8
10
12
0
1
2
3
4
5
6
7
8
−1
−1.2
−1.4
−1.6
−1.8
−2
−2.2
Position error bound [log(m)]

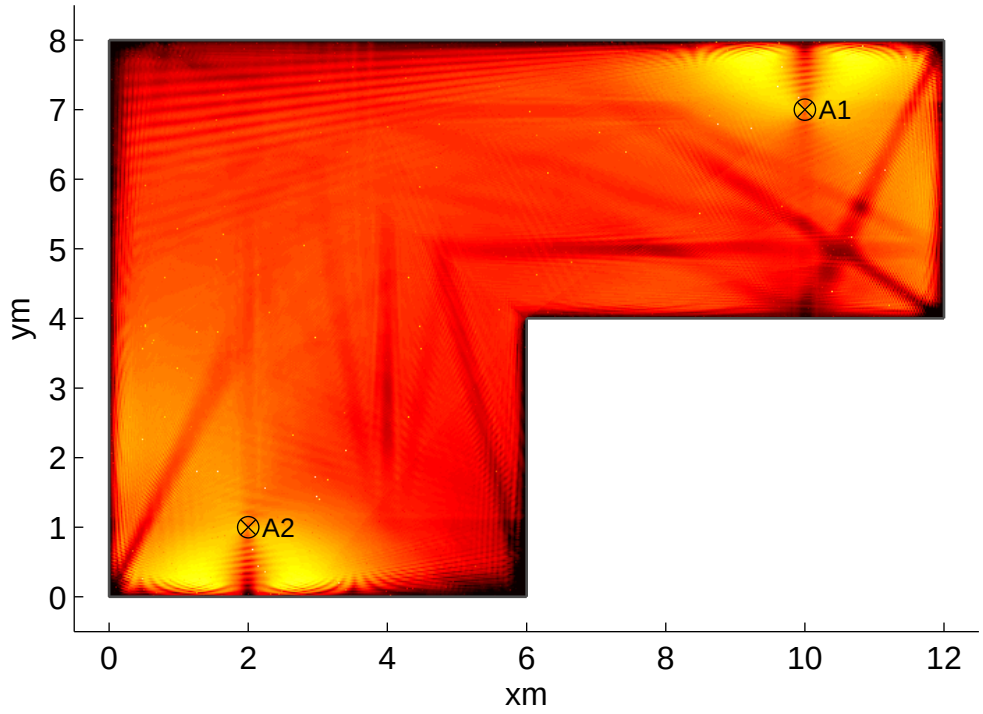
A1
A2
ym
xm
0
1
2
3
4
5
6
7
8
0
2
4
6
8
10
12

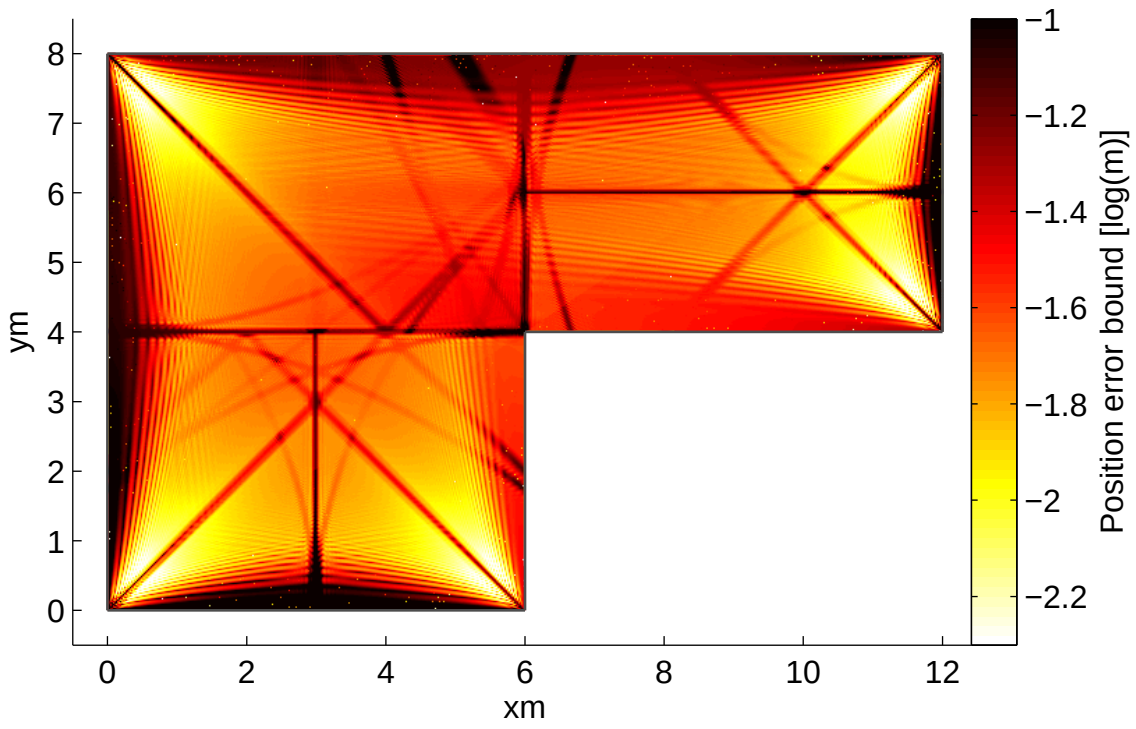
ym
xm
Position error bound [log(m)]
0
1
2
3
4
5
6
7
8
0
2
4
6
8
10
12
−1
−1.2
−1.4
−1.6
−1.8
−2
−2.2

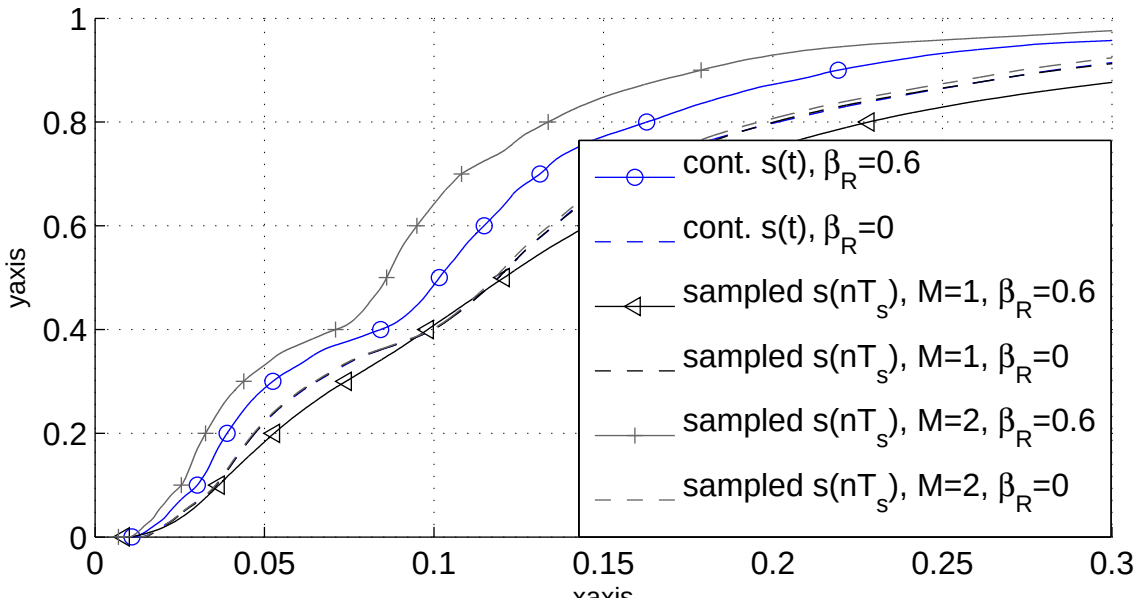
1
0.8
0.6
0.4
0.2
0
yaxis
0
0.05
0.1
0.15
0.2
0.25
0.3
xaxis
cont. s(t), β_R=0.6
cont. s(t), β_R=0
sampled s(nT_s), M=1, β_R=0.6
sampled s(nT_s), M=1, β_R=0
sampled s(nT_s), M=2, β_R=0.6
sampled s(nT_s), M=2, β_R=0

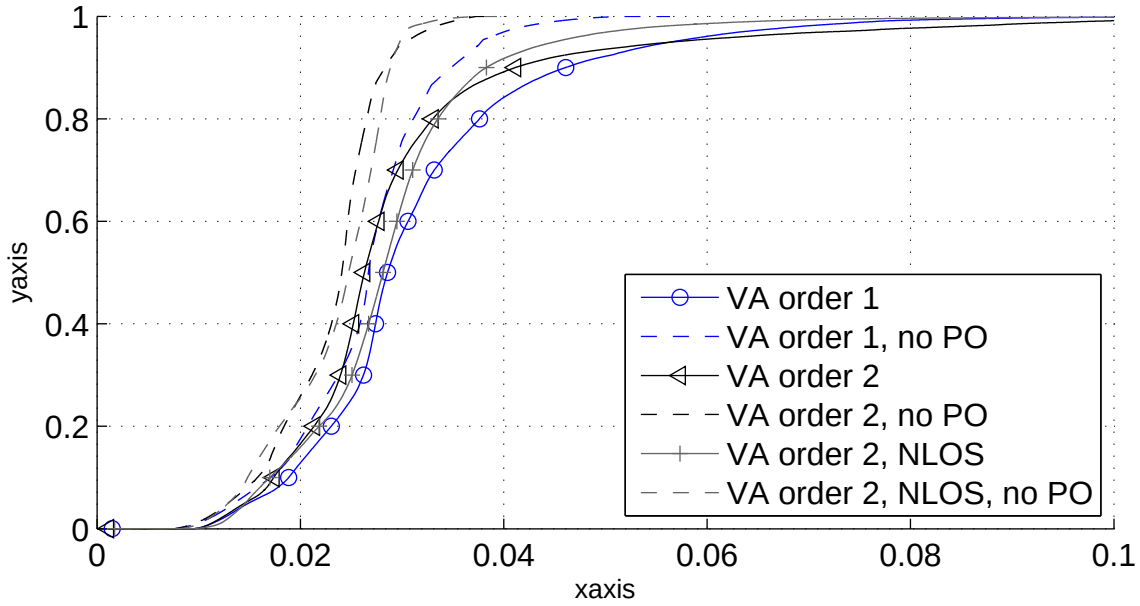
1
0.8
0.6
0.4
0.2
0
yaxis
0
0.02
0.04
0.06
0.08
0.1
xaxis
VA order 1
VA order 1, no PO
VA order 2
VA order 2, no PO
VA order 2, NLOS
VA order 2, NLOS, no PO

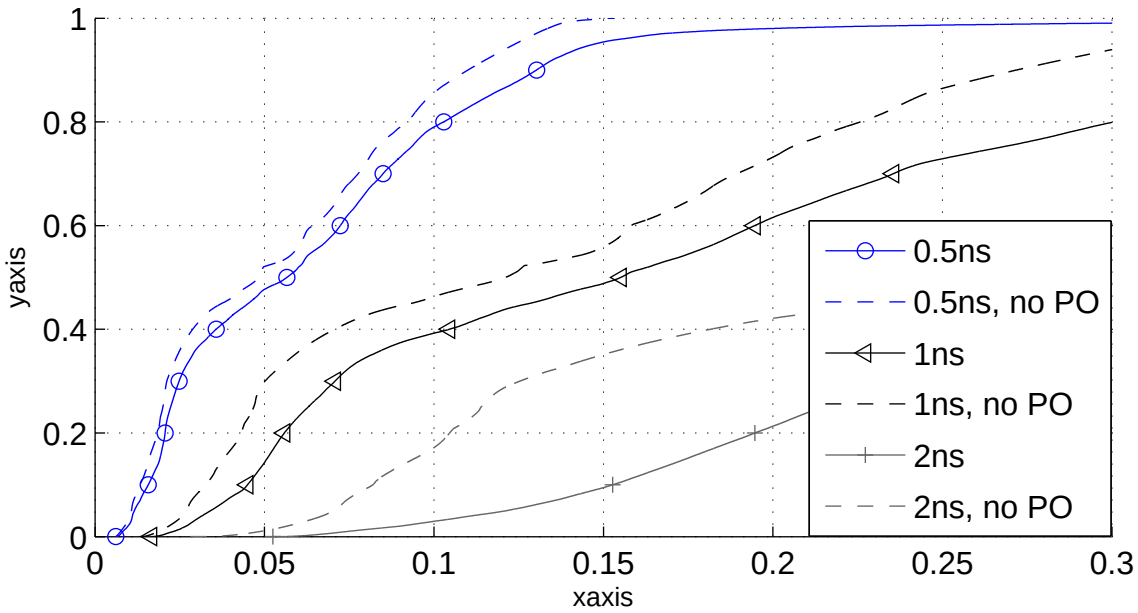
1
0.8
0.6
0.4
0.2
0
yaxis
0
0.05
0.1
0.15
0.2
0.25
0.3
xaxis
0.5ns
0.5ns, no PO
1ns
1ns, no PO
2ns
2ns, no PO

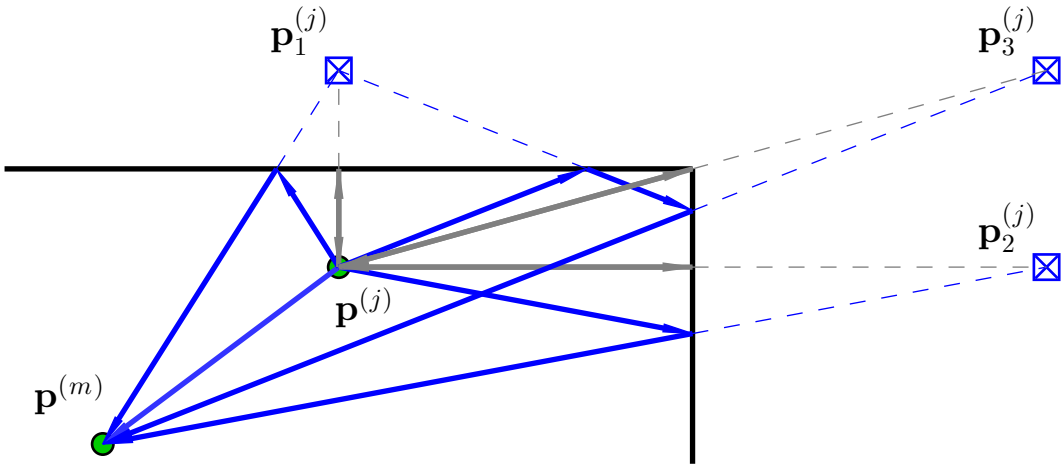
$\mathbf{p}_1^{(j)}$
$\mathbf{p}_3^{(j)}$
$\mathbf{p}_2^{(j)}$
$\mathbf{p}^{(j)}$
$\mathbf{p}^{(m)}$